Materials Characterization 163 (2020) 110298

Contents lists available at ScienceDirect

Materials Characterization

journal homepage: www.elsevier.com/locate/matchar

The effect of processing parameters on rapid-heating β recrystallization in inter-pass deformed Ti-6Al-4V wire-arc additive manufacturing

A.E. Davis[a,*], J.R. Kennedy[a], J. Ding[b], P.B. Prangnell[a]

[a] Department of Materials, The University of Manchester, Manchester M13 9PL, UK
[b] Welding Engineering and Laser Processing Centre, Cranfield University, Bedfordshire MK43 0PL, UK

ARTICLE INFO

Keywords:
Additive manufacturing
Titanium
Grain size
Recrystallization
Texture
Deformation

ABSTRACT

Relatively low levels of inter-pass deformation have been found to be very effective in refining the coarse columnar grain structures normally seen in Ti-6Al-4V components, built using wire-fed high-deposition-rate additive manufacturing processes. The most important process parameters that control the level of β recrystallization – the final grain size and micro-texture – were systematically investigated by simulating the deformation and high heating rate conditions in controlled samples, to develop the process knowledge required to optimise inter-pass deformation and obtain predictable grain sizes. Overall, it was found that the level of β-grain refinement achieved by inter-pass deformation was surprisingly insensitive to the ranges of deformation temperatures, deformation speeds, and changes to the as-deposited α + β microstructure, expected within the WAAM process window, provided a minimum plastic strain of only 14% was achieved in each added layer. Conversely, the final component grain size was shown to be strongly affected by rapid grain growth on reheating above the β transus. The texture results obtained were consistent with previous work which suggested that, with fine AM transformation microstructures, new β-grain orientations may be produced during the α → β transformation from the development of twinning faults, induced by the prior deformation and rapid heating. In contrast, greatly increasing the starting α lamellar spacing – to be more similar to that found in a wrought material – greatly reduced the level of recrystallization and also appeared to change the recrystallization mechanism to favour new β orientations produced largely by local lattice rotation.

1. Introduction

The α + β Ti alloy Ti-6Al-4V (Ti64) is widely used in the aerospace industry due to its excellent mechanical properties. However, it is expensive to produce wrought components from Ti alloys owing to the high processing costs involved [1,2]. Additive manufacture (AM) of Ti64 is therefore an attractive alternative, since the fabrication of near-net shape parts by AM technologies minimises the need for die tooling and final machining. Wire-fed, high power (> 2 kW) directed energy deposition (DED) AM processes are capable of efficiently producing parts with kilogram-per-hour deposition rates and build envelopes of several metres, which makes these processes particularly attractive for the manufacture of larger-scale aerospace components [3]. Such processes employ lasers [4], electron beams [5,6], or arc-plasma welding torches [7–12], as directed energy heat sources to deposit layers 1–2 mm thick. However, because of the larger melt pool dimensions, the solidification and cooling rates are considerably lower ($< 10^2$ °C s^{-1}) than experienced in powder bed technologies (10^{4-5} °C s^{-1}) [13–17] and as a consequence, components produced by high deposition rate DED can suffer from more severe microstructural heterogeneity and mechanical anisotropy [7,14,18]–[27].

Nevertheless, due to the higher cooling rates obtained by layer-wise deposition, relative to those achieved in heat treating bulk forged parts, as each deposition pass cools below the β transus temperature (~980 °C) in Ti64, the microstructure transforms to a very fine α basket-weave Widmanstätten structure, comprised of multi-variant α lamellar colonies separated by thin layers of residual β [18,19,22]. In comparison, in β-annealed forged wrought components, where the cooling rates are typically lower, the α basket-weave microstructure is generally replaced by coarser single-variant, grain-boundary-nucleated α colonies [2,28]. The α inter-lamellar spacing (ILS) and α colony size are controlled by the cooling rate through the β transus and decrease as the cooling rate increases, leading to a rise in yield strength, until it exceeds ~400 °C s^{-1} when the martensitic α′ phase forms which leads to a dramatic reduction in ductility [2,29]. In addition, in AM as each layer is deposited, repeated passes of the moving heat source give rise

* Corresponding author.
E-mail address: alec.davis@manchester.ac.uk (A.E. Davis).

https://doi.org/10.1016/j.matchar.2020.110298
Received 21 February 2020; Received in revised form 26 March 2020; Accepted 26 March 2020
Available online 28 March 2020

to steep thermal gradients and location-dependent cyclic heating that generates additional microstructure heterogeneity. This can cause rapid coarsening of the previously transformed α lamellae and increased α + β solute partitioning in the temperature range of the β approach curve (750–980 °C), creating distinct heat-affected zone (HAZ) bands within as-built deposits [18,19,22,27].

In moving melt pool process like AM DED, with Ti64, β-grain nucleation tends not to occur ahead of the solidification front due to the steep thermal gradients present in the heated melt pool and the minimal constitutional undercooling possible in the Ti-Al-V alloy system (Al and V both have partition coefficients close to 1 in Ti [30–32]); thus, columnar β grains generally grow epitaxially from the fusion boundary, which can continue to develop as each new layer is deposited and frequently grow throughout the entire build height to reach centimetres in size (e.g. [19]). The coarse columnar β-grain structures can also form a solidification texture, dictated by growth selection of grains preferentially aligned with their ⟨001⟩ direction normal to the solidification front, which typically generates a strong $\langle 001 \rangle_\beta$ fibre texture that is slightly tilted with respect to the build direction (ND) [13,20,33]. On cooling, this strong β texture determines the subsequent α texture that develops during the β → α transformation through the Burgers orientation relationship (BOR), which contributes to mechanical anisotropy, but is substantially diluted by the 12 possible α variant orientations [2,21,23,24].

More recently, the integration of an inter-pass cold deformation step into Wire-Arc AM (WAAM) has been demonstrated to be capable of refining the coarse-columnar β-grain structure, conventionally found in high deposition rate Ti64 AM, into much finer equiaxed grains, reducing both the coarse grain size and strong β and α textures [7,10,12,20,34–36]. Importantly, effective grain refinement was found to occur following the application of relatively low rolling strains, with an average layer-height reduction as low as ~8%, reducing the grain size by an order of magnitude [20,34]. This could be considered surprising as traditional processing of wrought Ti64 billets typically employs much larger strains (e.g. > 50%) to break-up the large β grains, although this is generally carried out at much higher processing temperatures due to the material's low ductility [37]. Donoghue et al. [20] have reported that average β-grain diameters of 140 μm and 94 μm can be achieved in WAAM deposits that were subjected to net layer height reductions of 8% and 19%, respectively, following inter-pass rolling, although no direct measurements of the plastic strains involved were made in this work.

In a more recent publication [35], the current authors found evidence that an unusually effective β-grain refinement mechanism may be operating in the deformed WAAM materials that involves annealing twining of β, which occurs due to growth faults forming as it re-grows on heating back through the α → β phase transformation. This mechanism was shown to provide many new β orientations; and in thermal simulations of deformed WAAM samples, produced an unusual microtexture within each original parent β grain, characteristically represented in $\{001\}_\beta$ pole figures by a four-pole motif, symmetrically centred on the parent grain ⟨001⟩ orientations. It was demonstrated that this texture could be replicated by double twinning of the {112}⟨111⟩ system. This explanation of the refinement mechanism was supported by in-situ-heating synchrotron X-ray diffraction experiments that simulated the WAAM cold rolling and heating cycle, in which the nucleation and growth of highly misorientated new β orientations were seen to consume all the prior parent β orientations in the last ~10% of the α → β transformation. A post-experiment electron backscatter diffraction (EBSD) scan also revealed that none of the prior parent β-grain orientations remained after the simulated WAAM heating cycle, again suggesting a twinning mechanism.

This high level of grain refinement was also shown to be highly heating-rate dependent, and only occurred under the rapid heating rate conditions found in AM processes [35]. This was postulated to be because the deformed microstructure recovered if heated too slowly so that heating rates intrinsic to DED AM processes, such as WAAM (~500 °C s^{-1} [22]), are uniquely suited to exploit this unusual type of recrystallization (RX) (henceforth referred to as *rapid-heating β RX*) [7,10,12,20,34,36]. It was also shown in our previous paper [35], that significant β-grain growth can occur during re-heating above the β transus, after the initial grain refinement had occurred [20]. In Ti64 WAAM [22,38], each layer is re-heated substantially above the β transus, so that grain coarsening is clearly a significant factor in controlling the final grain size in the WAAM process when inter-pass deformation is applied.

In WAAM deposited Ti64 material, to date, the β-grain growth kinetics have not been explicitly studied, although grain growth in conventional wrought Ti64 materials has been an active area of research. Work by Semiatin et al. [39] used an isothermal salt-pot technique to fit β-grain growth data in hot-rolled Ti64 samples heated between 1030 and 1090 °C to the classical law:

$$d^n - d_0^n = k(t - t_0)\exp(-Q/RT) \quad (1)$$

where d is the grain size as a function of time t, n is the grain growth exponent, k is a constant, t_0 is the time at which the steady-state temperature conditions had been reached, Q is the activation energy, R is the gas constant, and T is temperature. This study showed that β-grain growth in Ti64 was more rapid compared to in other metals, such as Al where there are stronger solute drag effects [40], and determined that $n = 2.0$, $Q = 312$ kJ mol^{-1}, and $k = 1110$ m^2 s^{-1} (with $d_0 = 40$ μm). However, the value for exponent n was considered unusually low, and the activation energy (Q) was higher than expected for diffusion controlled growth (e.g. for V). A more recent study [41] (also on hot-rolled Ti64 plates) reported that, at temperatures below 1250 °C, n can be as high as 4.6 and that texture strongly affected the grain boundary mobility. There is thus considerable variability in the fitting parameters reported for Eq. (1), which are greatly influenced by the texture and starting microstructure and may not, therefore, be appropriate for AM materials.

Since many factors can clearly influence the recrystallized β-grain structure obtained in WAAM Ti64 components when inter-pass cold deformation is applied, in the present work, we have sought to systematically investigate their relative significance so that the β-grain structure can be more reliably controlled when parts are produced under variable thermal conditions with more complex geometries. For example, to optimise inter-pass deformation to obtain the minimum and most uniform β-grain size, it is important to understand the effect of the key process parameters, such as the rolling reduction, strain-rate, and deformation temperature. Here, we have investigated their influence by varying the amount of deformation, deformation temperature, and strain rate, using plane-strain compression tests on WAAM starting material, followed by applying rapid heating cycles to simulate the re-heating step in WAAM inter-pass deformation, with accurately known conditions. In addition, the effect of the starting α microstructure, texture development, and β-grain growth were also investigated.

2. Materials and methods

Test samples were sectioned from a simple single-bead, 9 mm wide, linear WAAM wall built using Ti64 wire with a tungsten inert gas torch travelling parallel to the wall length, protected by a high flow-rate argon shielding device. The processing parameters are provided in Table. 1. A more complete description of the WAAM process is given in [7]. Small 5 mm^3 cube samples were sectioned from the steady-state region of the wall; i.e. the top and bottom 10 deposited layers were discarded [22]. Each sample contained 2–3 HAZ bands perpendicular to the build direction, and often had as few as 2 β grains parallel to the build direction, or consisted of a single β grain, all with a common $\langle 001 \rangle_\beta$//ND preferred orientation. A 6 mm wide α phase EBSD map, with the accompanying reconstructed β-grain structure taken across the centre plane of the WAAM wall, is shown in Fig. 1. It should be noted

Table 1
WAAM build parameters.

Wire feed speed	2.4 m min^{-1}
Travel speed	6 mm s^{-1}
Current	180 A
Interpass cooling time	30 s
Plasma gas flow rate	0.8 l min^{-1}
Tent shielding gas flow rate	8 l min^{-1}

that, since the samples contained very few β grains with a common ⟨001⟩ direction rotated around ND, the micro-texture that developed on deformation and re-heating the 5 mm^3 cube PSC samples could frequently be viewed as forming within a single parent β crystal.

Inter-pass rolling the top of a thin WAAM wall has been shown to produce an approximate plane-strain compression (PSC) [20], whereby lateral spreading occurs in the transverse direction and little elongation occurs in the wall length. To simulate these conditions, a PSC rig with a 5 mm wide channel was used (a schematic of the rig is provided in [35]) and the sample cubes were compressed in the build-height direction (ND), restricted by the channel walls in the heat source travel or welding direction (WD), and elongated in the transverse direction (TD). The samples were compressed in an Instron Universal Testing Machine with the channel die and samples pre-coated with a graphite-based lubricant. To simulate the inter-pass rolling conditions [42], most samples were compressed at room temperature, as rapidly as possible, with a crosshead speed of 0.5 mm s^{-1}, which will be referred to as the 'standard condition'. To explore the effects of deformation temperature and strain rate, samples were also deformed at 0.5 mm s^{-1} for temperatures up to 550 °C and at deformation rates down to 0.02 mm s^{-1}. At high test speeds, the sample reduction was difficult to control and could be ± 15% off-target. However, multiple tests were conducted to achieve a range of sample strains. Hot deformation tests were carried out in a Carbolite furnace with the same PSC tool pre-heated to the target test temperature. Samples were then inserted and compressed when at temperature, removed and air cooled outside of the PSC rig.

Finite element (FE) modelling was used to estimate the strain distribution within the PSC samples using the commercial software package QForm (Fig. 2). Material flow stress data for input into the model was taken from room temperature compression stress-strain curves of the standard Ti64 as deposited WAAM material (without inter-pass rolling). To model the friction, the Levanov friction equation [43,44] was used:

$$F_t = m\frac{\overline{\sigma}}{\sqrt{3}}\left(1 - exp\left[\frac{\sigma_\perp}{\overline{\sigma}}\right]\right) \quad (2)$$

where F_t is the friction stress, m is the friction constant, $\overline{\sigma}$ is the equivalent (Von Mises) flow stress, $\sigma_\perp$ is the normal contact stress, and n is the Levanov coefficient (in this case $n = 1.25$). Since non-symmetric barrelling occurred in the PSC tests (e.g. see Fig. 5), it was assumed that the PSC rig platen and channel had dissimilar effective friction properties, and m was fitted for each part by comparing the modelled to the actual sample shape changes. The final platen and channel friction coefficients used were $m = 0.65$ and $m = 0.085$ respectively. A series of example modelled sample strain distributions are shown in Fig. 2, for an increasing sample reduction.

The rapid heating experienced by each deposited layer in inter-pass deformed WAAM was simulated using induction heating in a TA Instruments DIL 805A/D/T quench-dilatometer. R-type thermocouples were spot welded to the centre of the 5 mm^3 sample ND-TD faces for temperature control, and the samples were heated at a rate of ~650 °C s^{-1} – which is representative of the WAAM process [22] – under vacuum. This heating rate was achieved using the dilatometer at 100% power for a predetermined time interval (~1.1, 1.2, and 1.3 s to reach target temperatures of 1100, 1200, and 1300 °C, respectively). As a result, once the target temperature was reached, the samples experienced some temporary instability (typically ± 20 °C) before equalising after ~0.5 s. To study the effect of the deformation conditions, all the samples were heated to a standard peak temperature of 1100 °C (~100 °C above the β transus) to ensure full transformation to the β phase field. For the grain growth experiments, samples were heated to a range of temperatures and isothermal hold times. Due to the sample shape, some non-uniform heating was expected; so, once at the desired temperature, the samples were held for a minimum of 1 s before

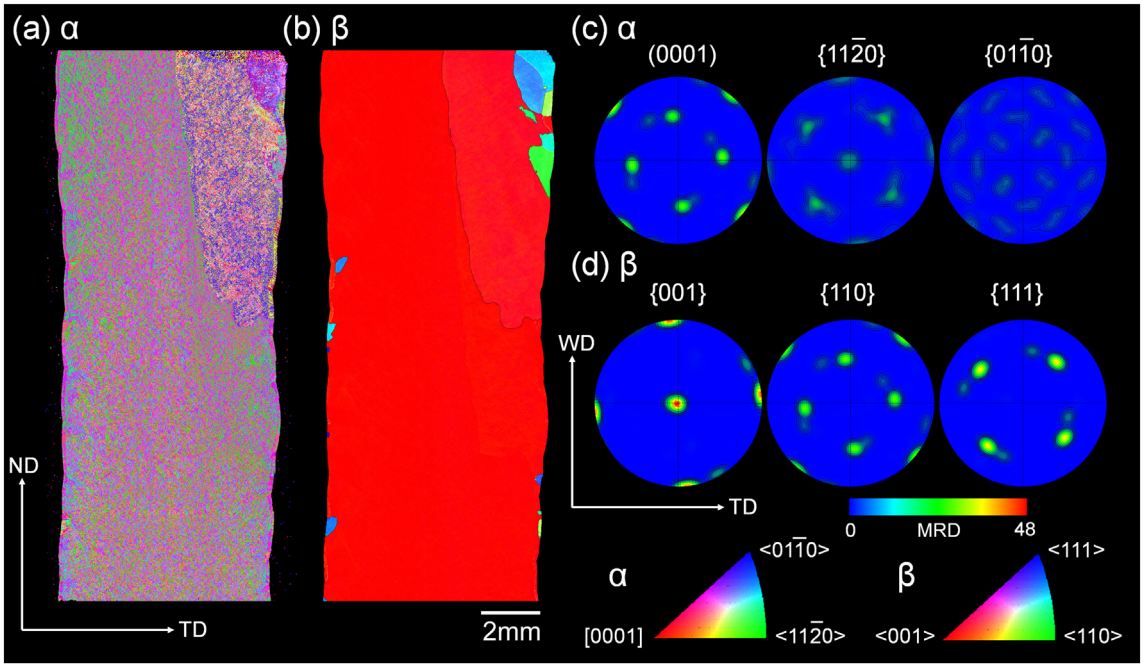

Fig. 1. Example microstructures and textures from the as-received WAAM material, taken across the centre of the wall (ND-TD plane): (a) α phase EBSD map, (b) β reconstruction of (a); (c) and (d) α and β pole figures, respectively. ND, TD, and WD refer to the normal, transverse, and welding (heat-source travel) directions respectively.

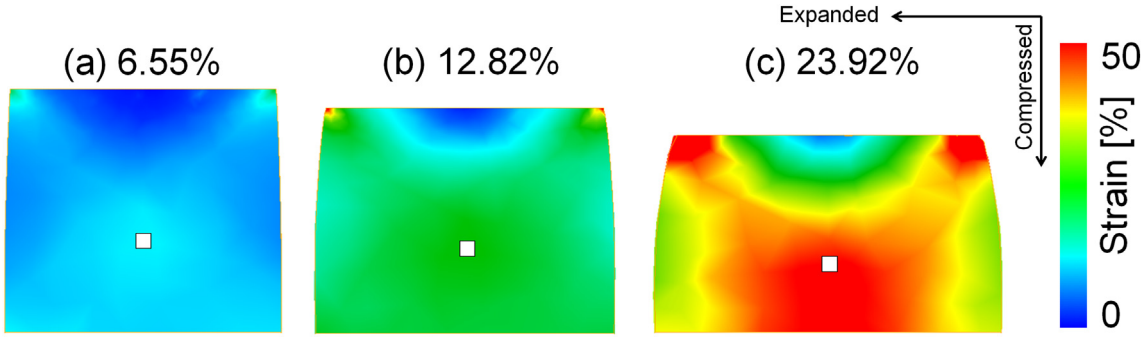

Fig. 2. QForm FE model simulations of the PSC samples deformed to varied strains, showing the predicted effective strain distribution in the samples with fitted friction conditions. Following β annealing treatments, strain estimates (taken from the marked points) were compared to the grain size measurements made at the same positions.

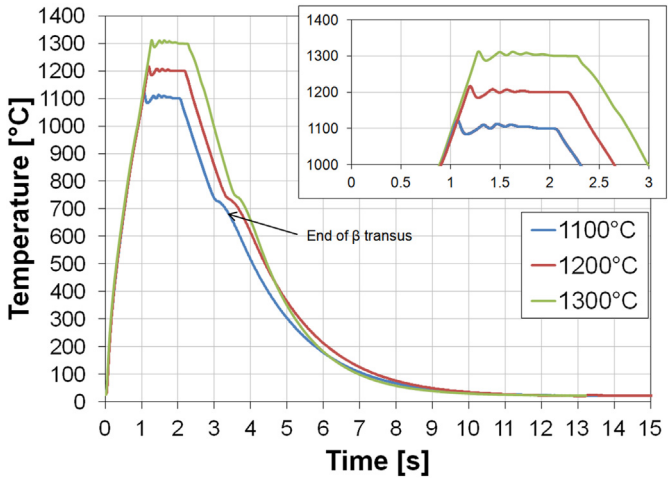

Fig. 3. Typical rapid heating profiles obtained for the PSC samples in the dilatometer. The magnified inset shows initial instability at temperature in the first ~0.5 s.

cooling to ensure the entire sample was at the target temperature and the grain sizes were always measured near the sample centre and thermocouple position. Following each heat treatment, the samples were force-cooled with He gas at a rate of 80 °C s^{-1}, unless otherwise stated. Typical heating profiles are provided in Fig. 3.

Analysis was performed by optical microscopy and SEM-EBSD mapping to determine the subsequent grain structure and textures. The compressed and annealed samples were sectioned in the centre ND-TD plane and prepared using SiC paper up to 4000 grit, followed by polishing using an OPS suspension mixed with 5% hydrogen peroxide, then etched in Kroll's reagent for optical observation. Optical macrograph maps were produced across the entire sample sections using a Zeiss M2 Imager, automatically over a pre-defined area, and stitched together to produce large, high-resolution images.

SEM backscatter micrographs of polished samples were taken on an FEI Sirion FEG-SEM at an accelerating voltage of 20 kV for low resolution images, and on an FEI Magellan FEG-SEM using an accelerating voltage of 5 kV for high resolution images. EBSD orientation mapping was performed on the Sirion SEM equipped with an Oxford Instruments' Nordlys Nano EBSD detector and AZtec acquisition software, using an accelerating voltage of 20 kV and a step size of 5 μm. Since the WAAM microstructures contained little and very fine residual β [22,26], to determine the β-phase texture and grain size β-phase EBSD maps were reconstructed from the α phase using the technique developed by Davies and Wynne [45,46] (based on [47,48]) where up to 2° of misorientation from a particular α variant was accepted, and a divergence of up to 3° from the BOR was considered to belong to the same parent β orientation. All EBSD maps are depicted in inverse pole figure colouring with respect to the build and compression direction (ND), and β-grain low angle grain boundaries (LAGBs, 5°–15°) and high angle grain boundaries (HAGBs, > 15°) are highlighted in white and black, respectively, unless otherwise stated. Grain sizes and texture data for β-phase pole figures were taken from the 2 × 2 mm central region of each PSC cube sample (unless stated otherwise), so that data was not skewed by the unrecrystallized sample 'dead zones'. Where multiple parent columnar β grains were identified in a PSC sample, the RX micro-texture was separated relative to each prior β grain (e.g. Fig. 12b). All pole figure intensities are scaled in multiples of random density (MRD).

Due to the high quantity of β-grain size measurements required from this large sample matrix, most measurements were made from optical micrographs using the linear-intercept method. Selected grain size measurements were also carried out in the Channel 5 software using EBSD maps to validate the optical measurements. Averages from both optical and EBSD map linear intercept methods were given 95% confidence intervals. The average initial α phase ILS was measured from SEM backscatter images, using the standard linear intercept method compensated for diagonally-orientated lamellae [26]. This measurement was averaged from 3 micrographs for a given sample condition and also given 95% confidence intervals.

3. Results

3.1. The effect of the deformation conditions on the recrystallized β-grain size

To obtain a broad overview of the effect of the process variables on the refined β-grain size seen that can be obtained with inter-pass deformation in the WAAM process, PSC deformation and rapid heating simulations were first conducted on a large matrix of samples to systematically vary the strain, strain rate, deformation temperature, and the starting microstructure prior to deformation. For all these samples, the β-grain size was measured after applying a standard simulated WAAM rapid heating cycle, with a low peak temperature of 1100 °C for 1 s. This heat-treatment ensured full transformation to β while minimising grain growth. It should be noted that the β-grain structure cannot currently be reconstructed from EBSD data from α phase that has experienced significant deformation, so it was not possible to study the 'as-deformed' β texture before recrystallization and re-transformation to undeformed α. All the processing parameters trialled, sample testing conditions, and starting α ILS measurements can be found in Table 2. The results from all these tests are summarised in Fig. 4, plotted as a function of the estimated strain (in ND) and the average grain sizes obtained are also provided in Table 2.

Table 2
Summary of the PSC test matrix and grain size results, providing the experimental deformation conditions: sample height reduction, estimated sample centre strain, deformation speed, temperature, starting α inter-lamellar spacing (ILS) before deformation; and the resultant average β-grain diameters. The grain sizes were measured optically using the linear intercept method, unless marked (*) where they were measured by EBSD, after the standard rapid β annealing treatment. The sample strains were estimated at their centre by FE analysis, except for the samples deformed at temperatures above 350 °C where they were estimated from the height reduction.

Experiment	Sample reduction [%]	Centre strain (ND) [%]	Deformation speed [mm s^{-1}]	Deformation temperature [°C]	Starting α ILS [μm]	Grain size [μm]
Effect of strain	5.95	9.26	0.5	~20	1.41 ± 0.07	278 ± 65
	6.55	9.84				130 ± 8*
	7.07	10.64				143 ± 11
	8.50	12.85				60 ± 4
	12.82	19.49				52 ± 3
	13.83	21.03				50 ± 2
	15.61	23.50				46 ± 3
	16.9	25.93				49 ± 16
	18.18	28.13				63 ± 4
	20.90	33.37				54 ± 3
	23.92	39.79				46 ± 1*
Effect of α ILS	15.99	25.60	0.5	~20	5.53 ± 0.28	~40*
	24.40	40.90			2.43 ± 0.55	43 ± 0*
	20.68	32.80			1.46 ± 0.33	56 ± 0*
	13.83	21.03			1.41 ± 0.07	41 ± 1*
	18.89	29.60			1.05 ± 0.06	45 ± 4
	17.38	26.60			0.62 ± 0.02	51 ± 0*
	16.77	25.90			0.76 ± 0.01	42 ± 0*
	18.02	27.80			0.44 ± 0.02	40 ± 0*
	15.17	23.40			0.23 ± 0.02	50 ± 0*
Effect of strain rate	18.18	28.13	0.5	~20	1.41 ± 0.07	63 ± 4
	18.38	28.90	0.2			55 ± 3
	16.94	25.90	0.02			59 ± 4
Effect of deformation temperature	23.92	39.79	0.02	~20	1.41 ± 0.07	46 ± 1*
	10.46	10.46		350		95 ± 6
	16.87	16.87		350		68 ± 4
	22.24	22.24		400		50 ± 3
	23.60	23.60		450		58 ± 3
	24.55	24.55		500		56 ± 5
	20.93	20.93		550		55 ± 3

3.1.1. *Effect of increasing strain*

PSC samples with the standard starting WAAM microstructure were deformed to reductions of 6–24%. Optical macrographs from a selection of these samples are shown in Fig. 5, which illustrates one of the limitations of PSC channel-die testing, in that the strain is concentrated in 'crossed' 45° shear zones and the sample centre. This non-uniform deformation is a consequence of tool-sample friction and difficult to eliminate in a PSC test, when testing a material with a low rate of strain hardening, despite careful attention being paid to lubrication. However, the FE analysis was used to aid interpretation by reducing the error in correlating the local deformation strain predicted for the sample centre to the microstructure. From the FE model, the corrected strains in the

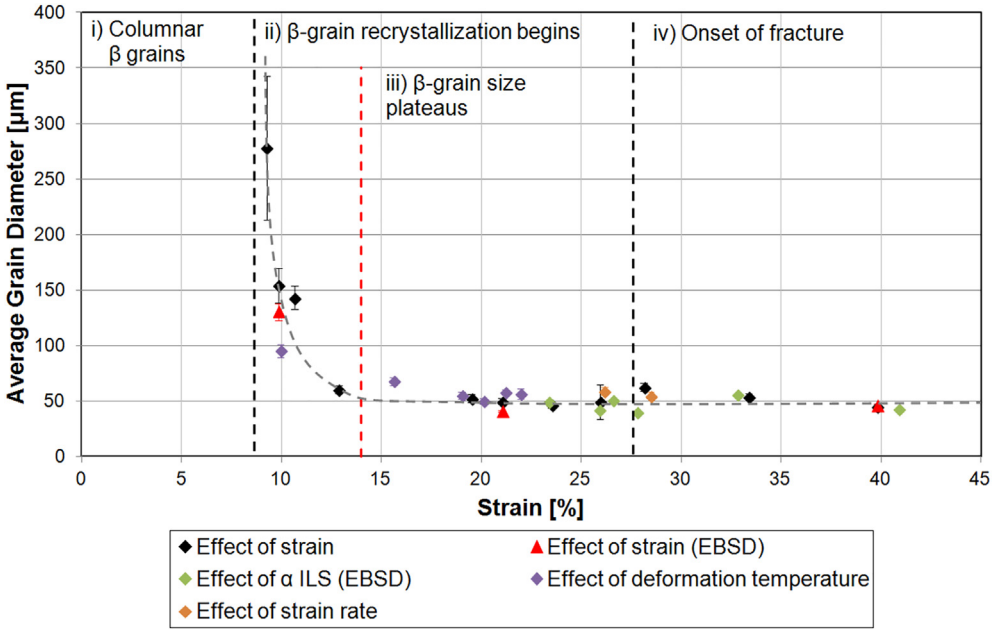

Fig. 4. Summary of the β-grain sizes measured from the PSC samples after the standard rapid WAAM heating cycle, plotted as a function of the local compression strain (in ND) estimated at the centre of each sample, where the grain size was measured. 4 different regimes are indicated where: i) the original columnar β grains still dominated; ii) the sample centre was fully recrystallized with equiaxed β grains which then rapidly reduced in size with strain; iii) where the level of grain refinement saturated; iv) where deformation was limited by the sample cracking. All grain diameters were measured by the linear-intercept method either optically or by EBSD. The sample conditions are detailed in Table 2.

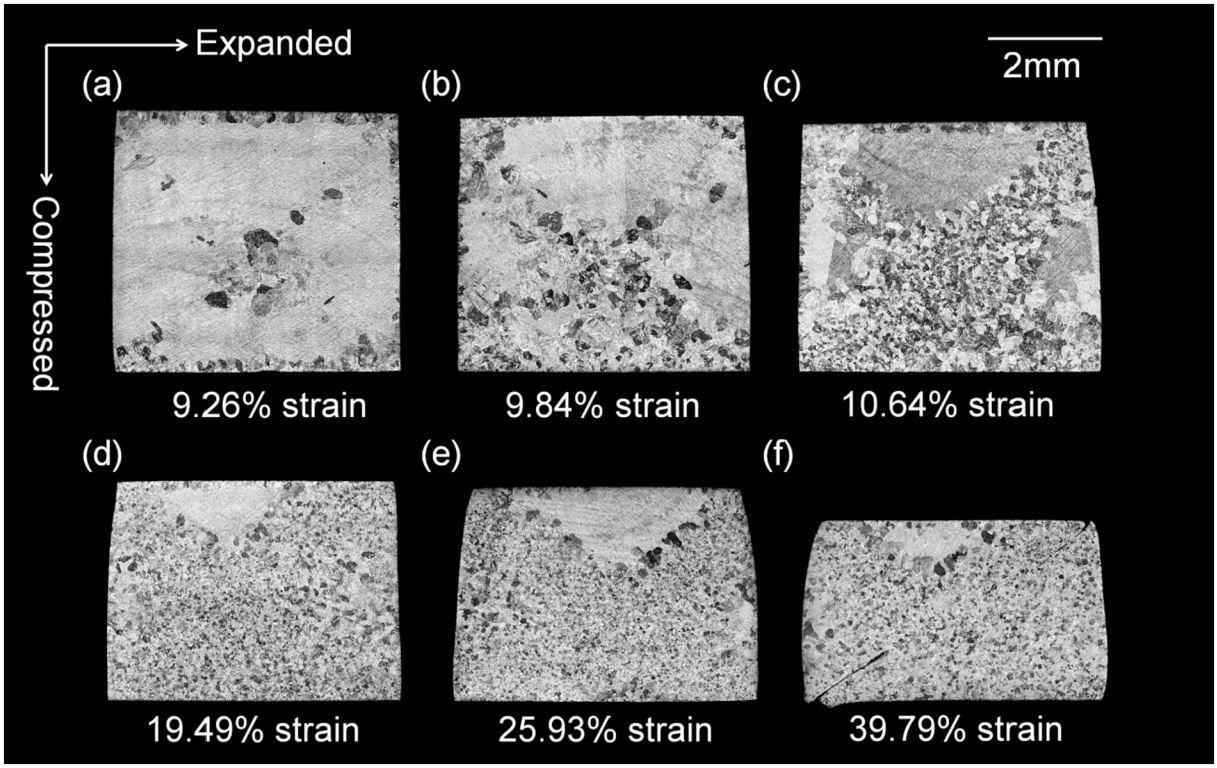

Fig. 5. Optical macrographs of PSC samples compressed to increasing strains. The 'strains' refer to the ND strain estimated at their centre using the FE model. All samples were deformed at room temperature and rapidly heat-treated at 1100 °C for 1 s.

central-recrystallized regions were estimated to be considerably higher at between 9 and 40%. The smallest reduction used, therefore, demonstrated that as little as a 9% strain in the sample centre was sufficient to generate some new β orientations and activate the rapid-heating β RX, as shown in the first sample in Fig. 5a. The requirement for only a small strain to achieve grain refinement is in good agreement with earlier work on WAAM inter-pass rolling in refs. [20,34] that found that recrystallization occurred for average layer height reductions of only 8%.

As the strain at the sample centres increased to ~14%, the β-grain size decreased to ~50 μm and the RX area grew, although unrecrystallized dead zones still remained at the sample left, right, and top regions (Fig. 5c and d); i.e. as the sample height reduction increased, the strain level required to generate new β-grain orientations spread throughout the majority of the sample. However, once the local strain achieved (predicted by FE) became greater than about 14%, no further β-grain refinement occurred and the grain size reached a minimum level of ~50 μm. Increasing the strain to 27% only saw further growth of the RX area into the sample 'dead zones'; i.e. the spread of plastic deformation led to further homogenisation of the specimen's grain structure, but no further reduction in grain size, and at higher strains, the samples began to fracture which provided an upper limit of the strain levels that could be achieved (e.g. Fig. 5f).

Thus, with increasing strain in the PSC simulations, the evolution of the recrystallized grain structure could be grouped into four ranges: i) 0–9% strain, where coarse columnar β grains inherited from the WAAM process remained and little or no RX was seen; ii) 9–14%, where many new β orientations appeared and there was a rapid reduction in the recrystallized grain size; iii) 14–27% strain, where the recrystallized grain size achieved a lower limit, but the sample volume that exhibited RX β-grain refinement increased as the strain level rose in the more constrained sample regions, which led to homogenisation of the grain structure; and finally, iv) > 27% strain, where the onset of cracking occurred. These regions are indicated in Fig. 4.

Overall, from these results, it is noteworthy that substantial β-grain refinement occurred after a low threshold strain of only ~9%, and saturated at a lower limit at a strain of only 14%, giving a constant recrystallized grain size of ~50 μm for higher deformation levels, despite the strain within the centre of some samples increasing to nearly 40% (Table 2). The minimum grain size obtained in these experiments of 50 μm was also consistent with the simulations conducted in our previous paper [35], as were the texture relationships found between the parent and new RX β grains formed after thermal cycling. The typical, but unusual texture behaviour is illustrated in Fig. 6 using pole figures obtained from reconstructed β EBSD maps where, due to the large original grains extending across the entire sample height (Figure 1), the prior parent β-grain orientations could be obtained from the sample dead zones. The textures depicted in Fig. 6 are from a sample deformed to a strain of 20% (at its centre) that had a single parent β grain at its centre before deformation and heating (conveniently orientated with ⟨001⟩ directions parallel to ND, RD and TD). By comparison of the 'before and after' pole figures, it can be seen that the new RX β-grain orientations exhibited the same unique micro-texture previously reported in [35] which, in the {001} pole figure, is characterised by a four-fold motif spread ~30° nearly symmetrically around the prior parent β-grain ⟨001⟩ poles. However, as will be discussed further below, for some deformation conditions greater localisation of shear in the PSC samples affected the texture development.

3.1.2. *Effect of deformation rate*

The standard deformation speed (of 0.5 mm s^{-1}) used for the majority of the samples was chosen, subject to equipment limitations, to be as close as possible to the actual WAAM inter-pass rolling process [7,10,34]. However, it was of interest to determine whether the strain rate had any effect on the rapid-heating β RX mechanism; thus, samples were also deformed to similar strain levels of 26–29% at slower deformation rates of 0.2 and 0.02 mm s^{-1} and compared to the original specimens deformed at 0.5 mm s^{-1}. Macrographs from these samples

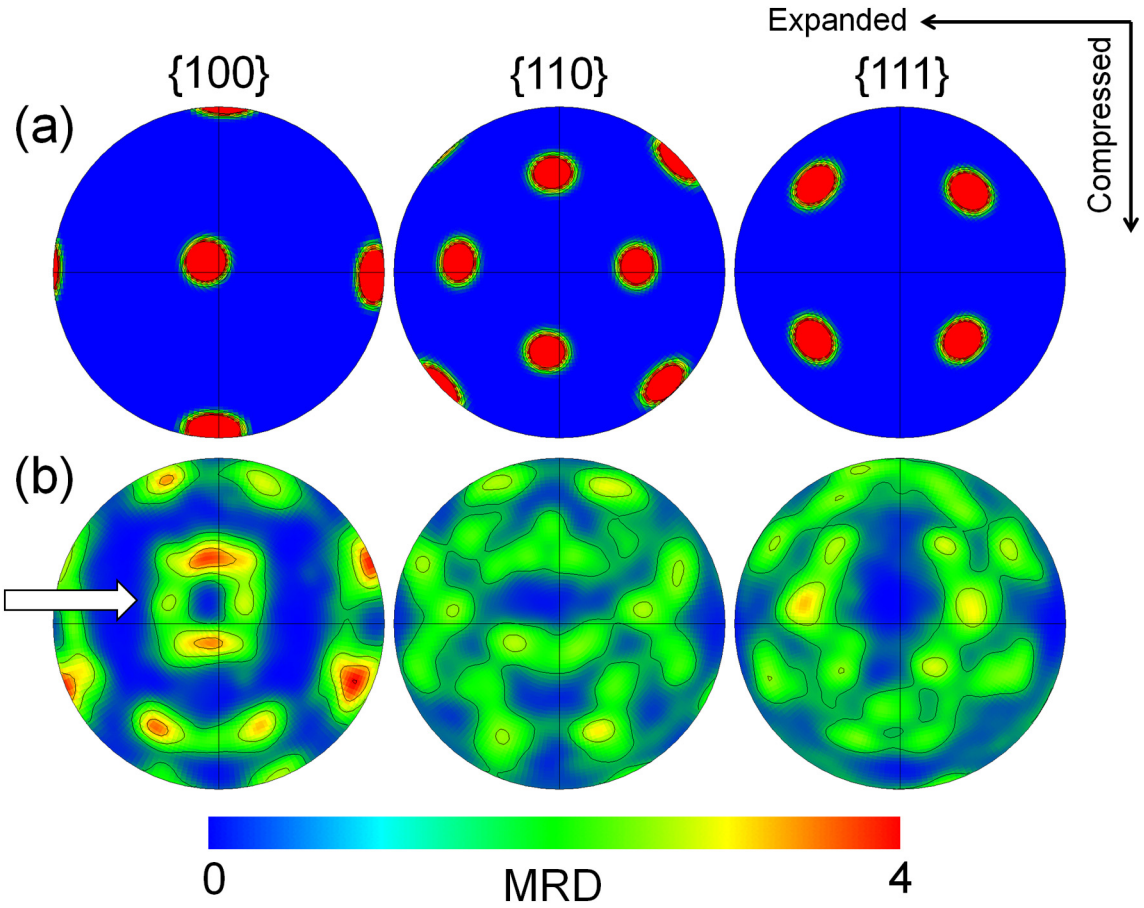

Fig. 6. Pole figures showing the typical 'before and after' texture for (a) the unrecrystallized prior parent β grain and (b) the RX β grains (reconstructed) that formed in the same grain, from a PSC sample, compressed to a height reduction of 14% (sample-centre strain estimated as 20%) under 'standard' conditions. Note: the characteristic four-fold motif centred on the parent grains ⟨001⟩ poles in the {001} pole figure for the recrystallized grains in figure (b) (arrow).

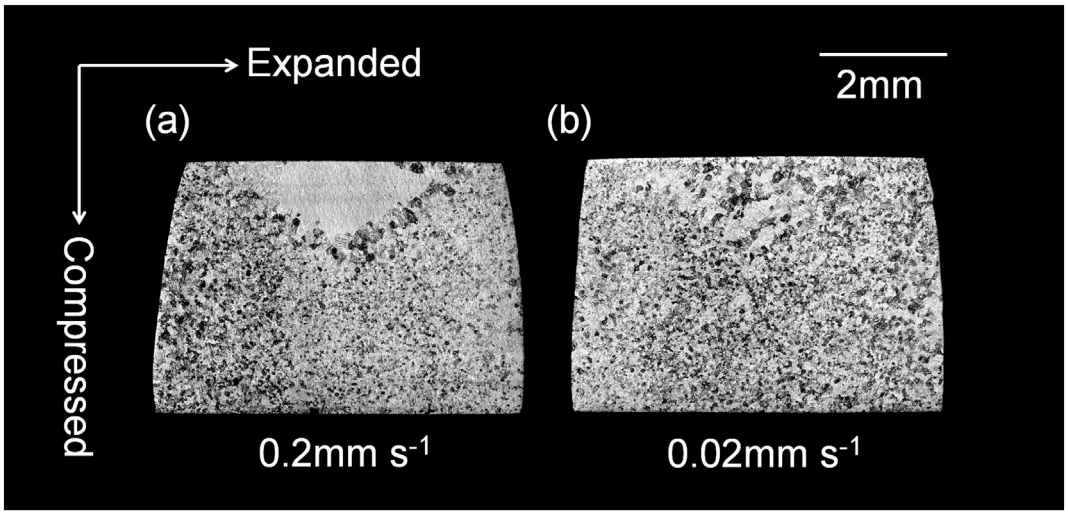

Fig. 7. Optical macrographs of PSC samples compressed at (a) 0.2 mm s^{-1} and (b) 0.02 mm s^{-1}. Both samples were rapidly heat-treated to 1100 °C for 1 s.

are depicted in Fig. 7, and their grain sizes are included in the summary plot in Fig. 4 and Table 2. Additionally, an EBSD map and {001} pole figure from the sample deformed at 0.02 mm s^{-1} at room temperature is provided in Fig. 8a. It can be seen from Table 2 and Figs. 7 and 8a, that the minimum β-grain size was largely unaffected by the change in strain rate, and the slower deformed samples also had measured recrystallized grain sizes at their centres of ~50 μm. However, the reduction in deformation rate to 0.02 mm s^{-1} did improve the homogeneity of the recrystallized grain structure in the PSC samples, suggesting that the lower strain rate promoted greater strain homogeneity. The {001} pole figures presented in Fig. 8a, taken from the centre of the slowest 0.02 mm s^{-1} deformation rate sample, also demonstrates that the micro-texture of the RX β grains was unaffected by the reduction in strain rate, with both the texture and intensities being similar to that seen in Fig. 6b.

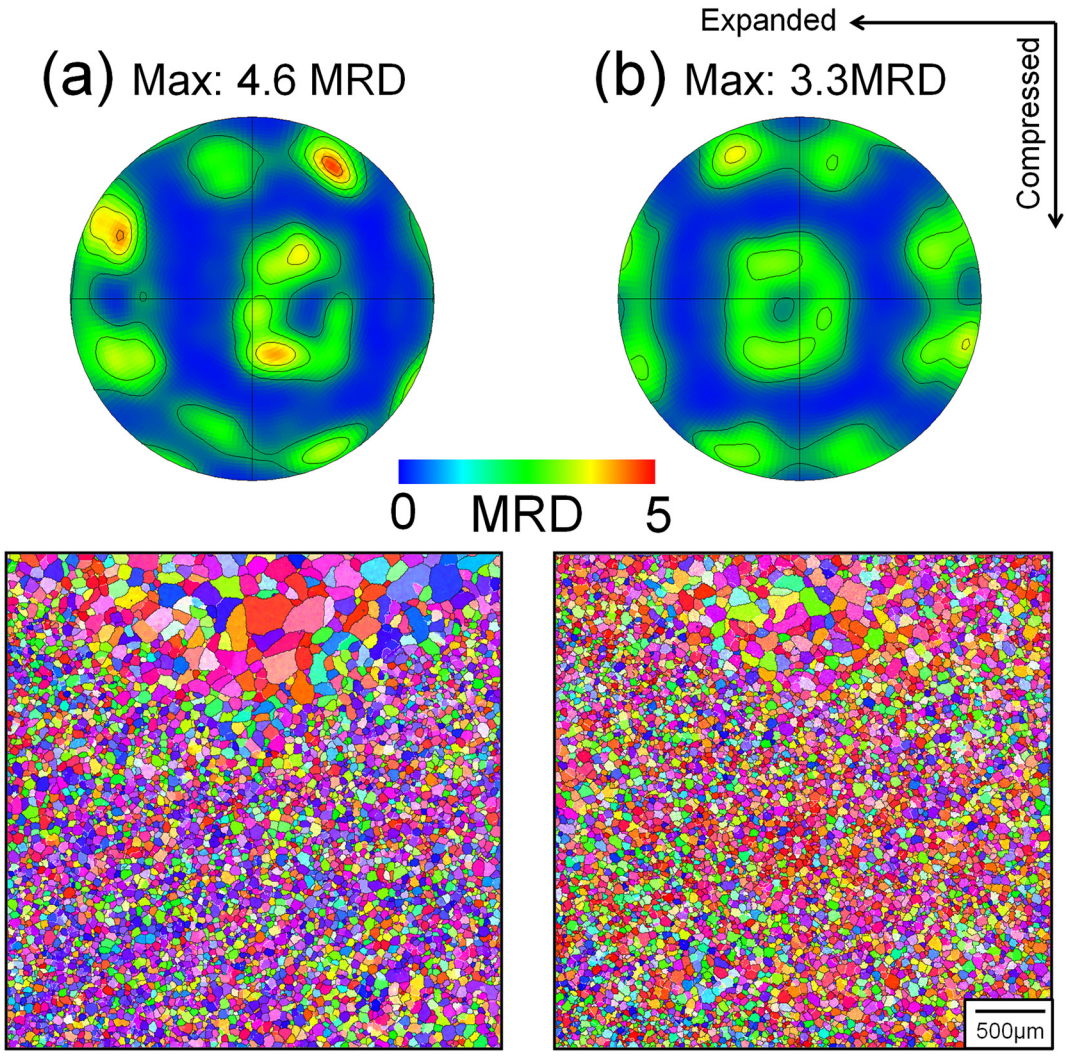

Fig. 8. Reconstructed β EBSD maps showing the RX grains at the centre of PSC samples and their accompanying {001} pole figures after deformation at (a) room temperature with a speed of 0.02 mm s^{-1} and (b) at 550 °C with a speed of 0.5 mm s^{-1}, then air cooled. Both samples were subjected to the standard rapid β anneal thermal cycle.

3.1.3. Effect of deformation temperature

All previous inter-pass deformation WAAM studies have been performed by waiting for the deposit to cool to near room temperature before applying the deformation step [7,10,34]. In the interests of reducing build times, the effect of the deformation temperature on the grain refinement efficiency was investigated; i.e. to see if the time delay before applying inter-pass deformation could be reduced without a detrimental effect on the level of β-grain refinement that can be achieved. To this end, samples were deformed at temperatures between 350 °C and 550 °C, a selection of which are shown in Fig. 9. For PSC sample reduction ratios of 20% or more (Fig. 9c–d), the β-grain size was again found to consistently reach the same minimum level of ~50 μm; i.e. deformation temperatures up to 550 °C appeared to have no effect on the maximum level of β-grain refinement achieved following rapid-heating β RX. However, samples deformed to lower strains of 11% and 17% reductions at 350 °C (Fig. 9a–b) were found to have larger β-grain sizes than those seen for samples deformed with comparable height reductions at room temperature (Fig. 5d–e). Following deformation at 350 °C and 550 °C, RX was also found to have occurred much more homogeneously throughout the PSC samples, suggesting strain was less concentrated within the shear zones and at their centre. The FE analysis that relied on room temperature material flow data was therefore assumed to have over-predicted the strain at the samples' centres. As a lower bound estimate, in the hot-deformed samples, the strain corresponding to the β-grain size measurements was therefore obtained from the sample height reduction (Table 2 and Fig. 4). When the β-grain sizes from the hot-deformed samples were plotted on this basis, in the summary graph in Fig. 4, their grain size measurements were still found to closely follow the trend for the room temperature deformed samples. Additionally, the EBSD map and {001} pole figure in Fig. 8b shows that, after deformation at elevated temperatures (at least up to 550 °C) and rapid-heating β RX, a similar characteristic micro-texture had again developed to that seen in the samples deformed at room temperature.

3.1.4. Effect of the initial transformation microstructure

The room temperature transformation microstructure can vary significantly in AM components due to differences in the cooling rate when α first forms, due to different deposition strategies. Long build durations can also result in an average increase in the α inter-lamellar spacing (ILS) within the bulk of a build due to thermal coarsening (e.g. [18,22]). It was therefore interesting to understand how variance in the α starting microstructure might affect the rapid-heating β RX behaviour seen in the WAAM samples subjected to simulated inter-pass deformation. To this end, a set of PSC samples were pre-heat treated by applying a short β anneal with cooling rates between 1 and 80 °C s^{-1}, to obtain a range of starting α microstructure scales with a different α ILS

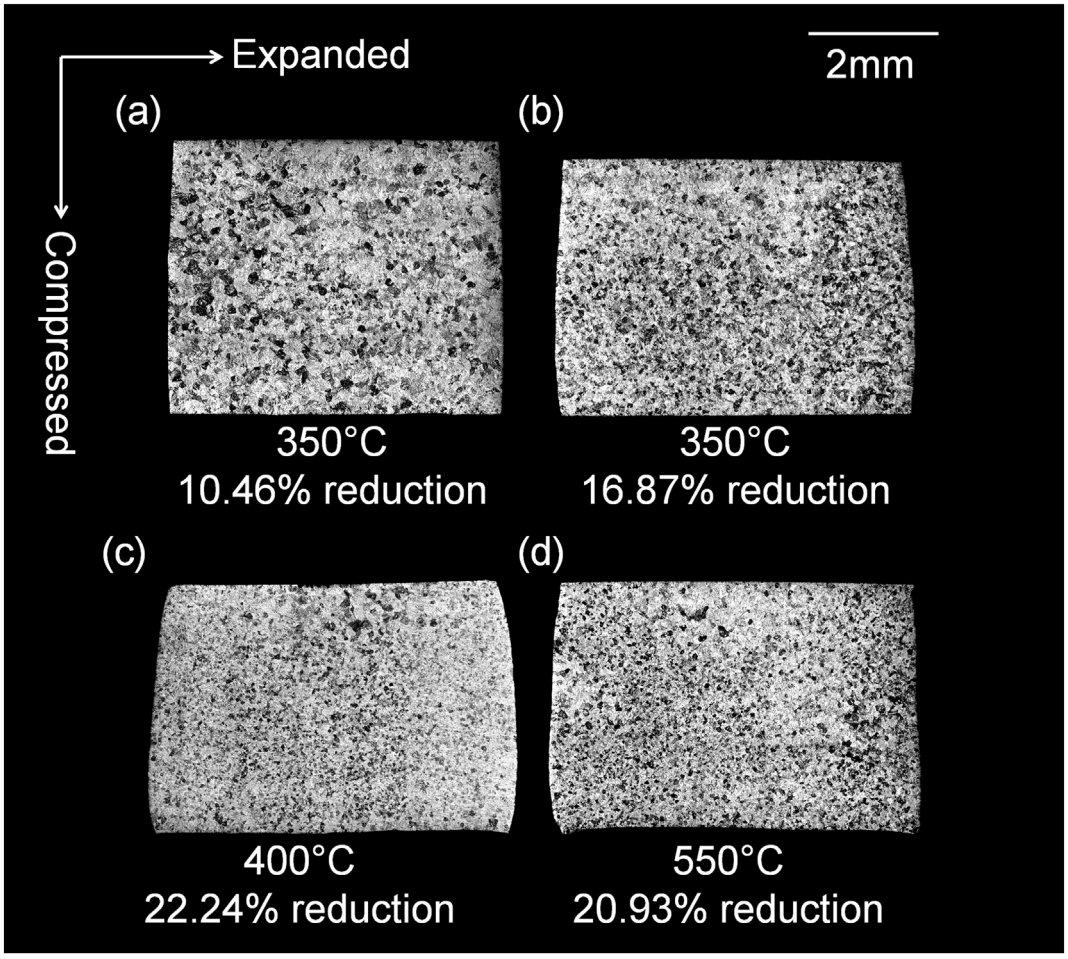

Fig. 9. Optical macrographs of PSC samples deformed at elevated temperatures, immediately air cooled, then rapidly heat-treated at 1100 °C for 1 s.

[2,14,21]. An additional sample was also cooled at a much lower rate of 0.1 °C s^{-1} to produce an α colony microstructure and a larger ILS of 5.5 μm, to replicate the coarser α microstructure typically found in a Ti64 forging following β annealing (e.g. [28]).

The change in α ILS for these samples with cooling rate are shown in Fig. 10a, where it can be seen that the α ILS achieved ranged from 0.2–5.5 μm, whereas in the standard WAAM material, it had an average spacing of ~1–1.4 μm. The samples were then deformed at room temperature to achieve strains of 21–41% at their centres (estimated by FE) and were subjected to the standard rapid reheating cycle (1100 °C for 1 s). The effect of their different starting microstructures on the rapid-heating β RX grain size and texture strength is summarised in Fig. 10b. It should be noted that, during deposition, the as-received WAAM material had experienced repeated thermal exposure below the

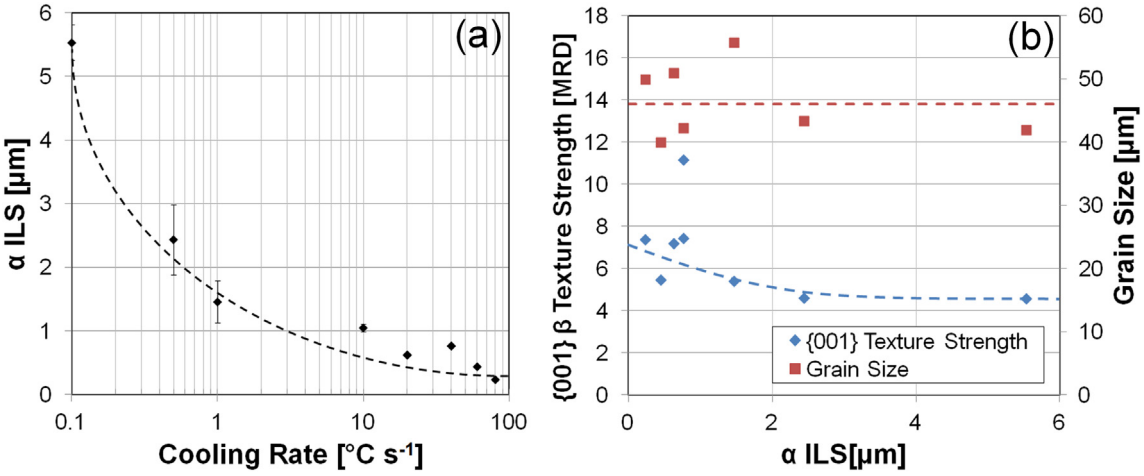

Fig. 10. The effect of the α inter-lamellar spacing (ILS) in the starting microstructure on the rapid-heating β RX grain size: (a) the α ILS achieved in the starting samples as a result of changing the cooling rate from a short β anneal, and (b) the effect of the α starting microstructure on the rapid-heating β RX grain size and {001} β texture strength after deformation at room temperature to a strain of 21% or above, in the centre of the PSC sample.

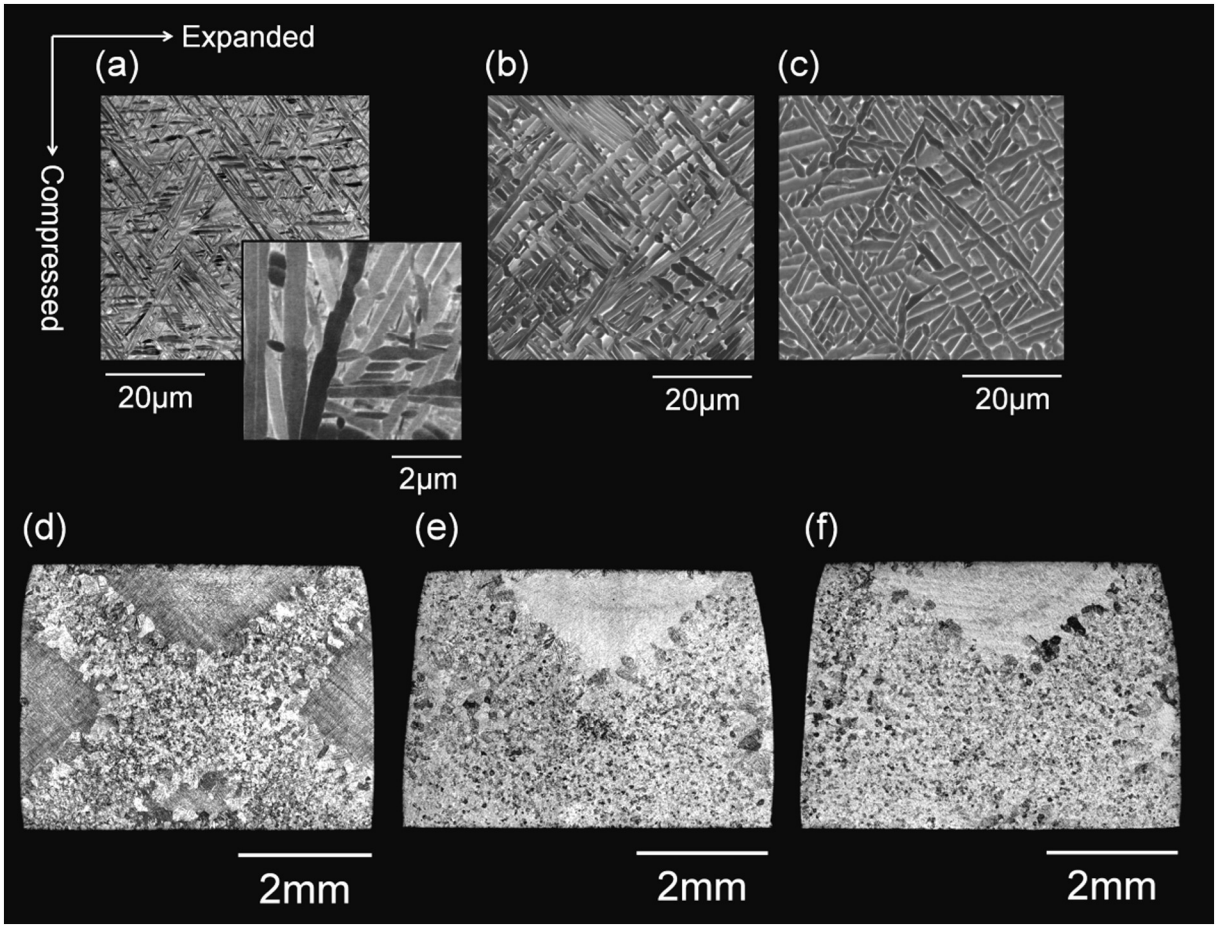

Fig. 11. SEM backscatter electron images of undeformed, β-annealed samples cooled at a rate of (a) 80 °C s^{-1} and (b) 40 °C s^{-1} (giving α ILS of 0.2 and 0.8 μm respectively), compared with (c) the as-received WAAM microstructure (with α ILS of 1.4 μm); below (d-f) are optical macrographs of the resultant β-grain refinement seen in the PSC samples after deformation and rapid heat treatment at 1100 °C for 1 s.

β transus, causing coarsening of the α lamellae, and so its ILS is not directly comparable to cooling rates of the β annealed and directly cooled samples.

Examples of different starting microstructures with initial α ILS of 0.2 and 0.8 μm (achieved by cooling at rates of 80 and 40 °C s^{-1}) are shown in Fig. 12a–b. The resultant RX β-grains seen in the corresponding, deformed, and thermally cycled PSC samples are provided in Fig. 11d–e and reconstructed β EBSD maps, with {001} pole figures, are presented in Fig. 12. These results show that the rapid-heating RX β-grain size was not greatly affected by increasing the starting α ILS in the range 0.8 μm to 2.4 μm, and rapid heating still produced an average grain size of ~50 μm in the centre of all the PSC samples. However, decreasing the starting α ILS spacing to 0.2 μm by increasing the prior-cooling rate (Fig. 11d) exacerbated the strain concentration and resulted in a more concentrated 'cross' 45° shear pattern and larger dead zones in the PSC samples. The RX β grains at the periphery of the crossed shear bands in this sample can also be seen (Fig. 12a) to have grown more obviously into the unrecrystallized deformed regions, suggesting that the dead zones were not strained enough to produce new β orientations and directional growth of the new RX grains that nucleated within the shear bands occurred into these regions.

To compare the above behaviour with that of a coarse α colony microstructure, more typical of a forging material, EBSD maps of the sample cooled at a much lower rate of 0.1 °C s^{-1} (α ILS of 5.5 μm) are provided in Fig. 13, where it can be seen that this sample behaved quite differently. Unfortunately, the less refined α + β microstructure of this sample also lead to premature cracking which limited the PSC sample height reduction to 16%. Nevertheless, the full sample EBSD map in Fig. 13b shows that, at its centre, after deformation and reheating, it contained mainly LAGBs with very few highly misorientated new β grains, and was comprised largely of finer subgrains. This behaviour is also highlighted in the enlarged maps in Fig. 13c–d. Some new RX β grains (with HAGBs) do, however, appear within the higher strain 45° shear bands where they have again grown outwards into the sample less-deformed regions. This behaviour, along with the greater tendency for cracking, suggests that the coarse starting microstructure resulted in fewer new grain orientations being generated and greater shear localisation within the 45° bands.

The central region of the coarse-α–colony β-annealed PSC sample shown in Fig. 13b contained two prior parent columnar β grains separated by a LAGB (arrowed), which can again be seen at its top (labelled 'β1' and 'β2'). Within the subgrain region shown in Fig. 13c, the texture for each prior parent β orientation can be seen to be different from that of the samples that started with a finer transformation microstructure, and consists primarily of a single component that is related to the parent grain orientation, but has become more spread and rotated. In addition, the characteristic four-fold symmetry motif seen in the higher cooling rate finer starting transformation structure samples is completely absent. From the pole figures, it can be observed that, within the shear zones, grain β1 (Fig. 13iii–iv) and β2 (Fig. 13i–ii) have rotated ~45° and ~30° about the PSC constraint direction (out of the page) and ~20° and 40° around the PSC extension direction, respectively. These large rotations suggest a greater strain actually occurred in the centre of the sample than in the specimens with more refined WAAM starting microstructures, but after exposing the deformed sample to the same thermal cycle, this did not result in anywhere near

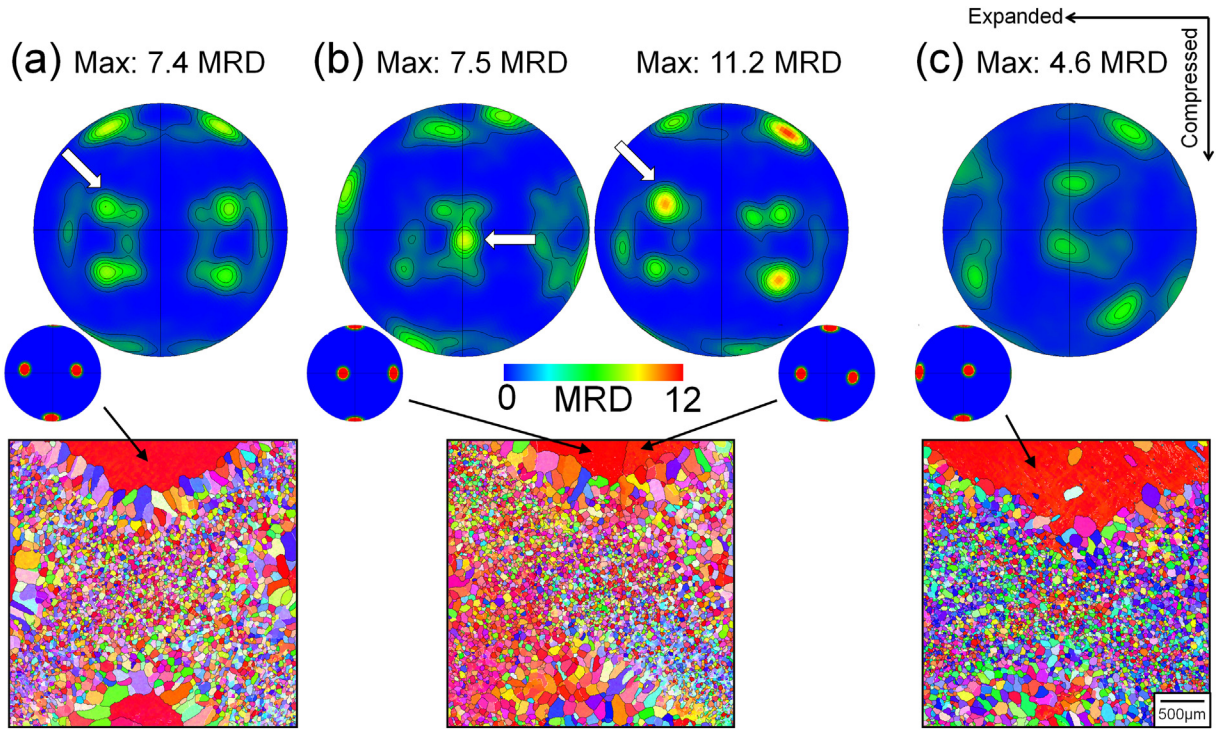

Fig. 12. Reconstructed β EBSD maps and RX-grain {001} pole figures for samples cooled at rates of (a) 80, (b) 40, and (c) 0.5 °C s^{-1} (corresponding to starting α ILS of 0.2, 0.8, and 2.4 μm respectively) after PSC deformation and rapid β annealing. Samples shown in (a) and (c) consist of a single parent β grain, whereas (b) has 2 parent β grains (with the boundary a little right of centre); separate pole figures are therefore provided for both RX regions corresponding to each parent grain in this sample. The arrows indicate stronger individual shear components present in the pole figures.

as many new highly misorientated β grains with HAGBs. However, further analysis of the micro-texture in the thin recrystallized regions in the 45° shear bands, where locally there were more highly misorientated grains present with HAGBs, did suggest that the characteristic rapid-heating β RX micro-texture was weakly present in parts of this sample. An example pole figure is shown in Fig. 13v, taken from the lower left shear arm at position (v). The texture motif is, however, less well defined than in the other samples that had finer starting structures (e.g. Fig. 6), although this could be due to the lower sampling statistics and the presence of the stronger rotated parent texture.

Following examination of the macro-texture in the sample deformed with a more conventional coarse starting transformation microstructure, it is worth returning to evaluate the texture in the other samples that had finer α ILS starting microstructures. Some of these samples cooled with the highest cooling rates (80 and 40 °C s^{-1}) also showed stronger single components that distorted the more ideal characteristic four-fold symmetry motif seen in Fig. 6 (arrowed in Fig. 12). For example, the sample in Fig. 12b, with an ILS of 0.8 μm (which was cooled at a rate of 40 °C) contained 2 prior parent columnar β grains, mutually rotated about a common ⟨001⟩ ND axis, before deformation and subsequent β rapid-heating and RX. This can be seen from the pole figures taken from the unrecrystallized dead zones at the sample top. The pole figure EBSD data for this sample has been consequently divided into halves, to separate the RX micro-textures seen within each prior parent β grain. It can be seen that this procedure has again revealed the four-pole motif, noted above, centred on the parent grain {001} orientations, but with a less symmetric intensity distribution. This is partly due to the reduced statistics, but also because of the overlap with a single stronger component, which probably has a similar origin to that seen for the coarse microstructure sample in Fig. 13, in that it was formed by rotation of the parent orientation due to the more intense shear localisation.

Closer examination of these single component orientations showed that they dominated in the PSC sample's 45° shear zones. To investigate this further, one shear arm of the highest cooling rate sample, with an ILS of 0.2 μm (Fig. 12a, cooled at a rate of 80 °C s^{-1}), was mapped at higher resolution by EBSD (Fig. 14a). The dominant texture orientation seen in the β {001} pole figure was separated and plotted in a further map displayed in Fig. 14c, and the pole figure for this texture component is shown in Fig. 14ii. This strong orientation can now be seen not to be part of the characteristic rapid-heating β RX texture motif, but instead has been caused by the more intense shear localisation that occurred in this sample, owing to its fine starting microstructure, which has rotated the parent grain orientation locally, similar to that seen in Fig. 13. This effect of increased shear localisation with a finer prior α microstructure, and the associated local lattice rotation, may also have caused the increase in recrystallized texture maximum strength reported in Fig. 10b; where reducing the α lath spacing gave rise to the appearance of stronger single shear components within the texture data.

To summarise: varying the scale of the starting α transformation microstructure only affected the rapid-heating β RX response significantly when it was coarsened to a level much more than that normally seen in material produced by an AM process. The RX β-grain size (defined as β grains with HAGBs) was largely unaffected by the starting microstructure when the α ILS was 2.4 μm or lower, although when decreasing the α ILS to this range, more shear strain concentration occurred in the PSC samples, producing a smaller refined region; and this was also associated with a rise in texture strength, due to the presence of some single shear components. In contrast, when a very slow prior cooling rate of 0.1 °C s^{-1} was used – similar to that experienced in a β annealed forged material – to obtain a much coarser starting lamellar α microstructure (ILS = 5.5 μm), a significantly different β-grain structure was observed, whereby the central more deformed region became dominated by subgrains, instead of the highly misorientated RX β grains with HAGBs seen in the samples that had a fine starting α microstructure, more typical of AM. In addition, the texture of this sample also changed and was more conventional, being

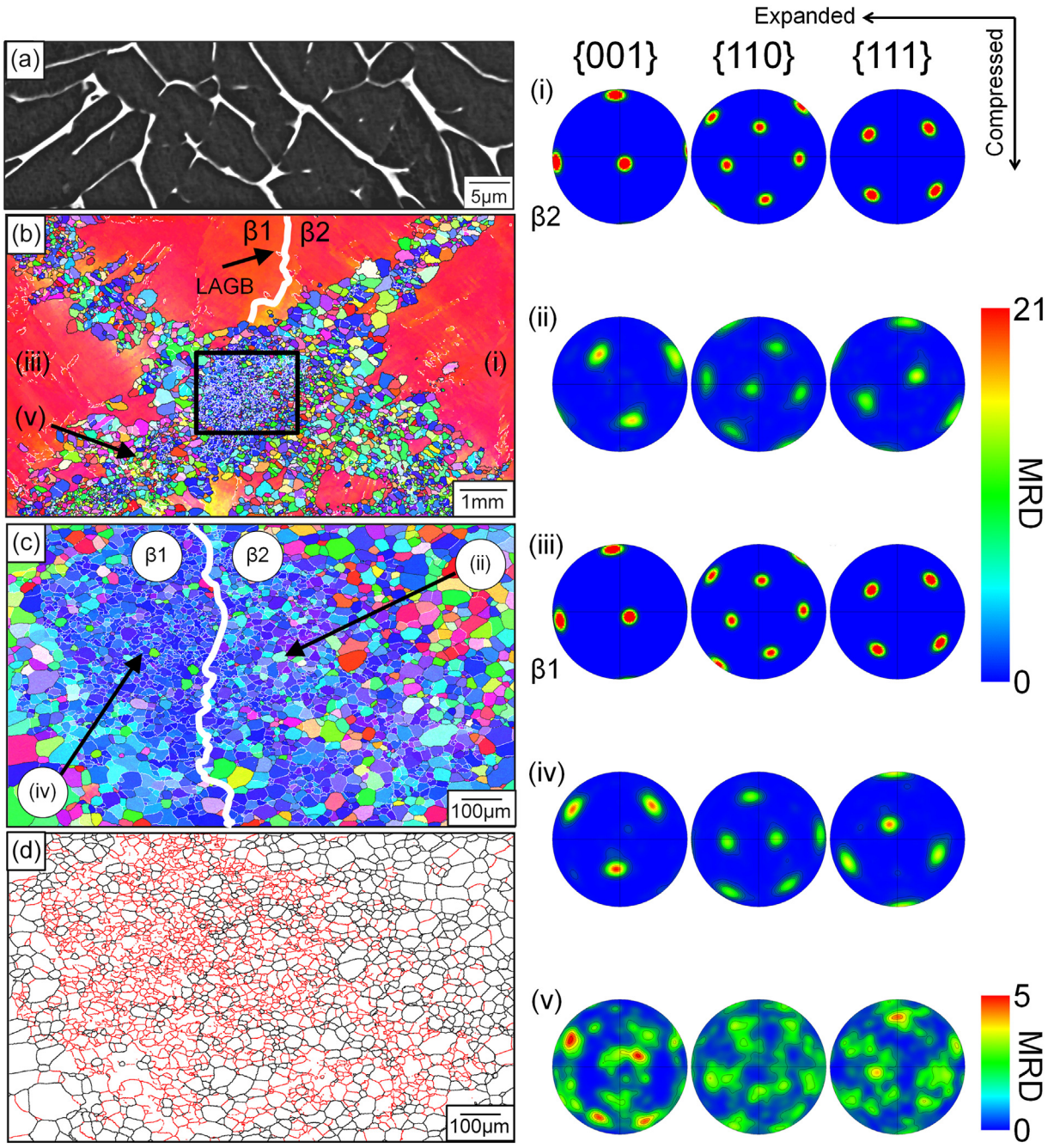

Fig. 13. The rapid-heating β RX behaviour of the sample cooled at a slow rate of 0.1 °C s^{-1}, to replicate a β-annealed forged material's transformation microstructure, before deformation by PSC: (a) SEM image showing the coarse microstructure before deformation; (b) reconstructed β EBSD map after PSC deformation and rapid heating showing the whole sample, the centre of which is magnified in (c); (d) depicts HAGBs and LAGBs within the parent β grains, coloured black and red respectively. Pole figures (i) and (iii) display the reconstructed β micro-textures from the large columnar parent grains, (ii) and (iv) show their respective textures in the central deformed and sample region; (v) provides an example of the minority texture component which is reminiscent of the unique motif associated with the rapid-heating β RX mechanism (e.g. Fig. 6). (For interpretation of the references to colour in this figure legend, the reader is referred to the web version of this article.)

dominated by shear components that exhibited single rotations with respect to a given parent grain orientation. This replaced the unique four-fold texture motif that was consistently seen in samples, which had fine starting transformation microstructures.

3.2. β-Grain growth

In WAAM and most other AM processes each deposited track experiences a complex thermal history, where the material is re-heated with a diminishing peak temperature above and below the β transus multiple times (e.g. [22]). Following deposition of a layer and applying an inter-pass deformation step, when the next layer is deposited, the temperature in the previously deformed layer will reach to the material's melting point, and as well as recrystallization, this would be expected to cause significant β-grain growth despite the short time experienced above the β transus. Similar effects have also been widely seen near the fusion boundary on welding fine grained wrought Ti alloys [49]. It is therefore important to characterise the grain growth response, as it probably limits the grain size reduction possible in an inter-pass deformation AM process.

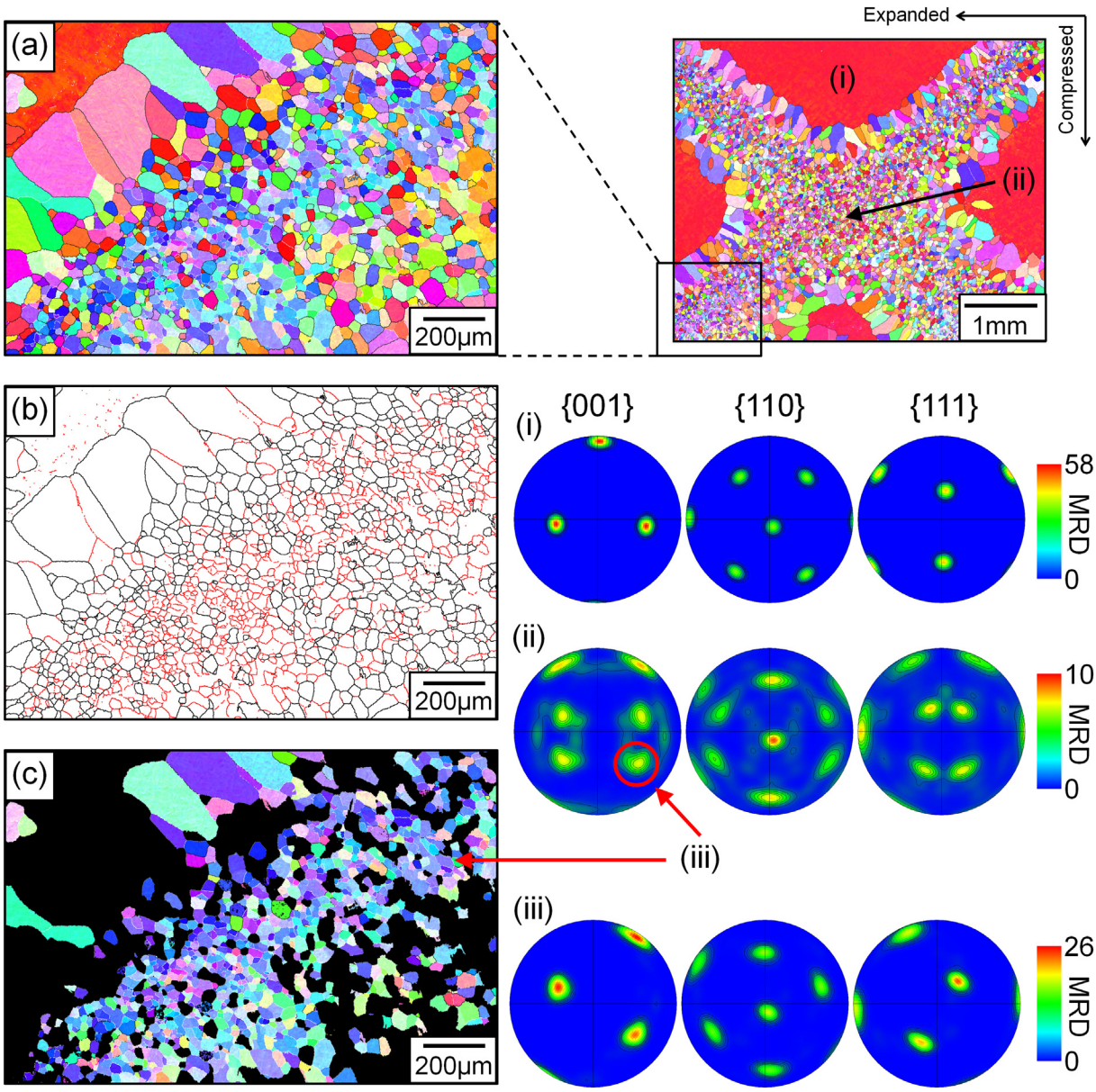

Fig. 14. (a)–(c) higher resolution EBSD maps from the PSC shear arm highlighted in the sample in Fig. 12a which had a very fine transformation microstructure (α ILS = 0.2 μm) before deformation and rapid heating: (a) displays the β reconstruction of the shear arm, (b) shows the β boundary character in this region (HAGBs and LAGBs are coloured in black and red respectively); and (c) has been filtered from (a) to include only grains with the single texture component highlighted in (ii), the pole figure of which is shown in (iii). The pole figures in (i) displays the texture of the prior parent columnar β grain, (ii) the micro-texture data taken only from the central RX β-grain region, and (iii) the separated shear component.

To initially assess the potential extent of grain growth, standard WAAM material PSC samples were deformed at room temperature to reductions between 16 and 19% and rapidly heated to up to 1300 °C for 1 s, and then quenched with He. These samples were then compared to those previously heated to 1100 °C, following PSC deformation with a comparable strain (shown in Figs. 5 and 6). In Figs. 15a–c and 16a and c, it can be seen that the increase in peak temperature to 1300 °C enlarged the β-grain size by over 80%, and produced a notably more homogeneous grain structure within the PSC samples. After heat treatment at 1100 °C, less-deformed zones were still found at the top, left, and right of the PSC samples, where the local strain was not high enough to produce RX, which was concentrated within the 45° shear bands and towards the sample centre. In comparison, following treatment at 1200 °C and 1300 °C, the highly misorientated new grains, that formed within the more heavily deformed shear regions and centre of the sample, spread outwards and consumed the less-deformed regions. Reconstructed EBSD maps from these samples (Fig. 16a and c) show the β-grain structures more clearly, and further demonstrate the stability of the characteristic rapid-heating RX β-grain texture; i.e. even after substantial grain growth there is little change in the original RX texture and the same four-fold motif can be seen, symmetrically centred on the parent ⟨001⟩ poles in all the {001} pole figures, as noted after the lower temperature 1100 °C rapid thermal cycle shown in Fig. 6b.

Further samples were also heat treated isothermally at 1100 °C, 1200 °C, and 1300 °C for up to 32 s to study the β-grain growth kinetics, and a summary of the β-grain growth behaviour is provided in Fig. 17. During the 1–32 s hold at 1100 °C, the β grains grew by 270%; whereas at 1200 °C and 1300 °C the grains grew less rapidly by 214% and 145%, respectively, over the same time period. In addition, it can again be seen from the pole figures in Fig. 16 that the even more extensive grain growth found for these longer exposure times equally had little effect on the RX β texture, which maintained the same characteristic intensity

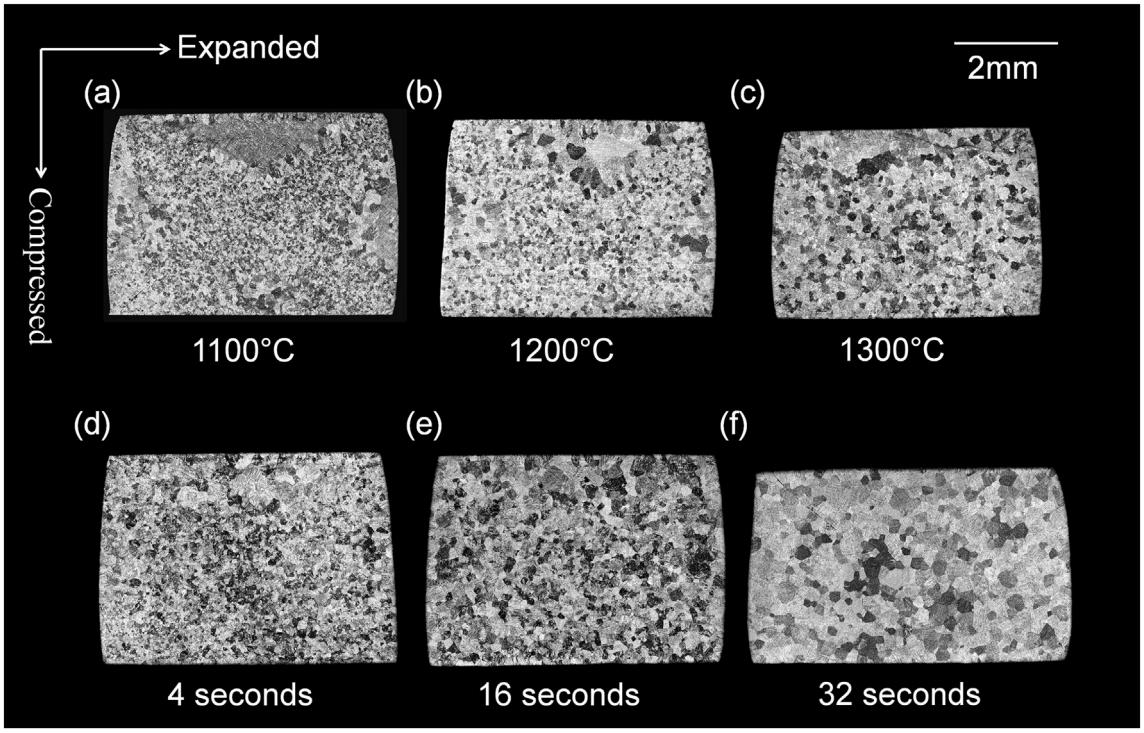

Fig. 15. Optical macrographs of PSC samples deformed under standard conditions and rapidly heated for 1 s at (a) 1100 °C, (b) 1200 °C, and (c) 1300 °C; and samples heated to 1100 °C and held isothermally for (d) 4 s, (e) 16 s, and (f) 32 s.

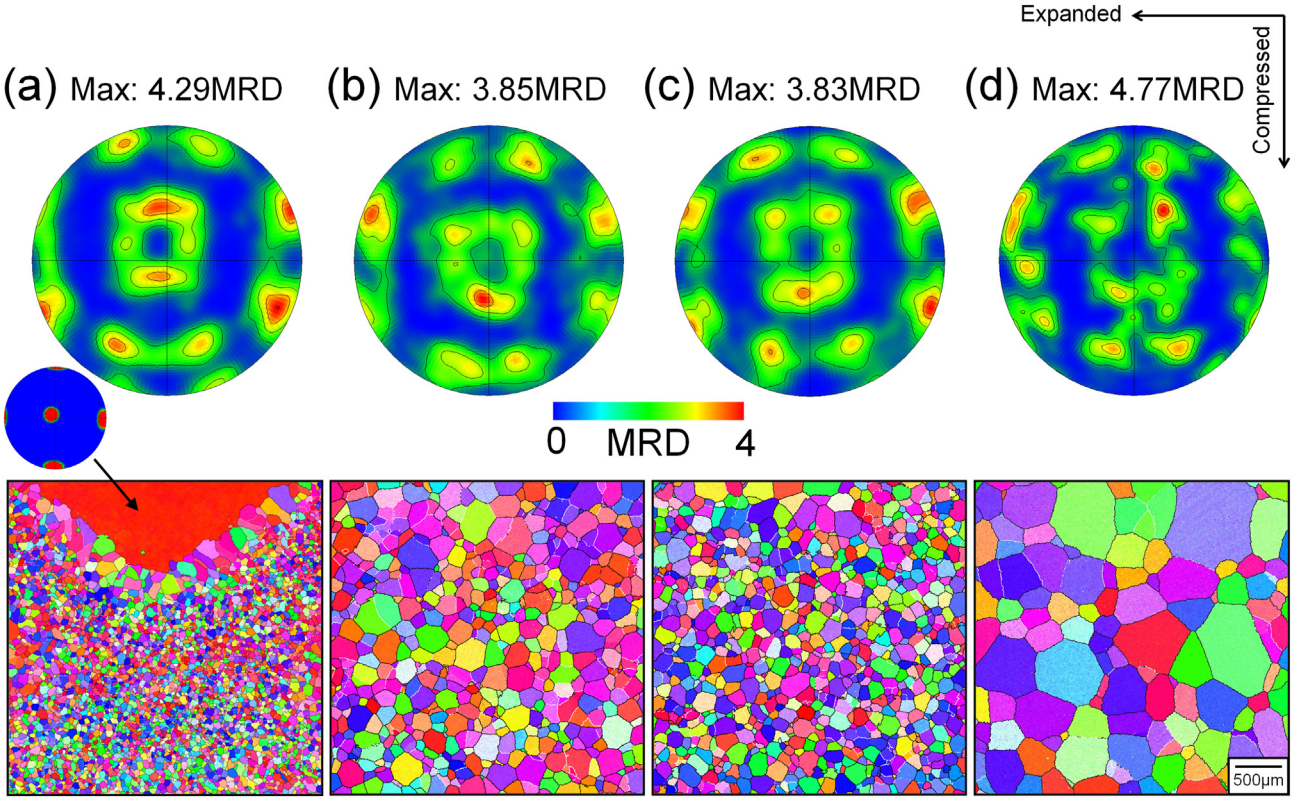

Fig. 16. Reconstructed β-phase EBSD maps and RX-grain {001} pole figures from deformed PSC samples (standard conditions) after rapidly heating to (a) 1100 °C for 1 s, (b) 1100 °C for 32 s, (c) 1300 °C for 1 s, and (d) 1300 °C for 32 s.

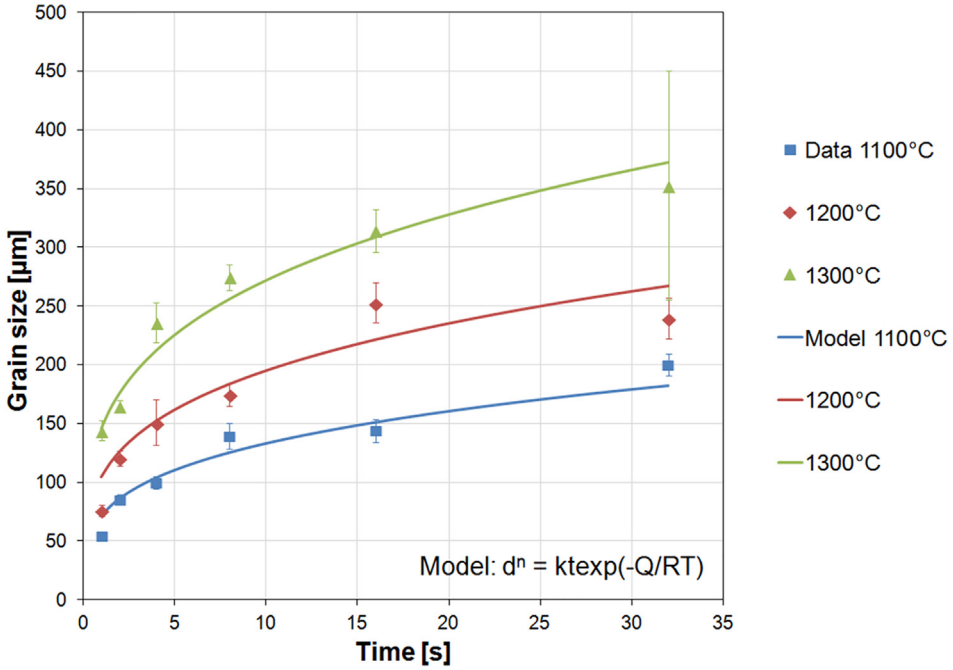

Fig. 17. Summary of the β-grain growth measurements performed for 3 peak temperatures (points) fitted with Eq. (1) (lines).

distribution. However, it should be noted that discretisation started to occur in the ⟨001⟩ poles for the sample heat treated at 1300 °C and held for 32 s (Fig. 16d) owing to the large β-grain size.

4. Discussion

When inter-pass deformation is applied to an added layer in the Ti64 WAAM process, the rapid re-heating cycle experienced during deposition of the subsequent layer has been found to lead to RX of the large columnar β grains normally formed by solidification [20,34]. It has been shown that the high level of grain refinement and reduction in texture strength that can be achieved by taking advantage of this cyclic in-situ deformation and heating process can reduce anisotropy, and improve the mechanical properties of WAAM components [7,12,20,34]. It has further been noted that substantial β-grain refinement can be obtained with the application of a relatively low plastic strain to each layer (> ~10%) [20,34]. Previous research [35] has investigated this behaviour with WAAM-equivalent simulated deformation and heating rate conditions, combined with detailed in-situ studies. This work concluded that the RX mechanism responsible for this beneficial effect could involve the development of new β-grain orientations by annealing twinning, which occurs specifically in lightly deformed, fine, WAAM transformation microstructures, on re-growth of the β phase during rapid heating through the β transus. A characteristic feature of this mechanism is the appearance of an unusual micro-texture that, in {001} pole figures, produces a characteristic four-fold motif symmetrically centred on the parent ⟨001⟩ grain orientations, with all the original orientations lost after annealing; i.e. in a recrystallization texture of a lightly deformed metal, it is more normal to see a spread of orientations from the original parent orientation. This micro-texture was again consistently seen here in the samples deformed with the standard WAAM starting microstructure (Figs. 6 and 8) and in the grain growth experiments (Fig. 16), but was not seen in the sample that had a much coarser starting transformation structure, similar to that found in a β-annealed forging.

In prior work, other sources of new grain orientations have also been noted on re-heating cold-deformed WAAM microstructures associated with prior β-grain boundaries, where local lattice rotation occurs from plastic compatibility during deformation [35]. This alternative source of new grain nuclei would be expected to be more important at higher strains and in materials with coarser colony microstructures, where it can also occur at colony boundaries [2,40]. It should also be noted that in the actual inter-pass rolled WAAM process, the cyclic repetition of straining and re-heating each layer does not allow as coarse a columnar structure to develop as we used for our starting material. However, these samples were used because the main focus of the work was to establish the limiting process parameters that controlled the onset of RX in a WAAM deposited material, and this also allowed us to analyse the 'before and after' behaviour seen on deforming and annealing single parent β grains. Experimentally, this was achieved by simulating the deformation using PSC samples with a wider range of strains and more control than is possible in the actual WAAM inter-pass rolling process, starting with the worst case scenario of a coarse-grained, columnar, WAAM deposited material (produced conventionally) and then replicating the rapid re-heating that occurs within the WAAM process with an accurately known thermal cycle.

An experimental difficulty in this approach was the non-uniform straining behaviour of the PSC samples. This is unfortunately a common problem with compression testing and a consequence of tool-sample friction in the PSC channel die tests, which is difficult to eliminate, despite careful attention being paid to lubrication. FE analysis (Fig. 2) was therefore used to reduce the error in correlating the sample strain to the microstructure. However, it was found that the non-uniformity of the strain in the PSC samples tended to increase with very fine transformation microstructure samples, and in the very coarse lamellar sample, which had a stronger tendency for shear localisation; whereas shear localisation diminished with lower strain rates and at higher deformation temperatures.

4.1. Effect of the process parameters on β recrystallization

Taken together, the results have shown that, after applying a standard rapid heating cycle with a low peak temperature above the β transus (1100 °C), the level of grain refinement achieved was surprisingly insensitive to all the parameters studied, which were selected to cover the range of relevance to the WAAM inter-pass deformation process. This included variance in the scale of the starting transformation microstructure, strain rate, and deformation temperature. The

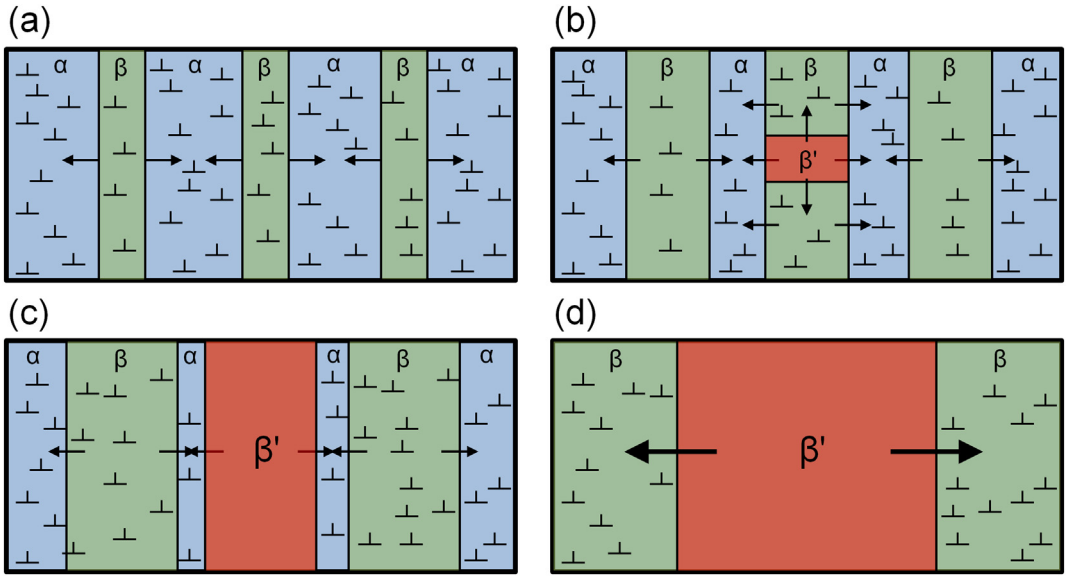

Fig. 18. The proposed mechanism responsible for the β-grain refinement in a lamellar α + β microstructure: (a–b) with a small sample strain, during rapid heating, stored dislocations in the microstructure nucleate a single annealing twin in the residual β with a new orientation (β′), which grows into the neighbouring deformed β while it is still pinned by the transforming α (c); then, in the final stage of the phase transformation, β′ grows into the remaining deformed β to dominate the microstructure (d).

latter parameter was limited by the PSC tooling to 550 °C, but during a large WAAM build, inter-pass rolling would typically be applied after completing each layer, where the residual surface temperature would not be expected to be at a higher level.

In agreement with our previous work [20,35], it was confirmed that only a low applied strain was required to activate β recrystallization in a WAAM material when subjected to a rapid re-heating cycle (Fig. 4). Recrystallization initiated when the local strain (estimated by FE analysis) in the PSC sample centres reached above only ~9% and, after the α → β transformation, this was sufficient to produce a microstructure consisting of many new highly misorientated β-grain orientations with HAGBs. With increasing prior strain, the average RX β-grain size (measured for boundaries > 15° in misorientation) decreased to a lower limit of 50 μm, and then rapidly plateaued at a low strain of ~14–18%, following which, it remained constant within the strain range achievable before the samples started to crack in the PSC test (up to ~40%). This behaviour is consistent with the annealing twining mechanism previously proposed in [35] and summarised in Fig. 18, in that to form the high density of highly misorientated nuclei necessary to generate this level of grain refinement in a coarse-grained material, a much greater plastic deformation would be required to generate sufficient local lattice rotations and there would be expected to be a more progressive reduction in grain size with strain [40]. An alternative explanation is that cold deformation produces deformation twinning, or that sufficient shear localisation occurs in a fine basket-weave microstructure that is also able to generate many new highly misorientated β orientations at low applied sample strains. In our previous study, we were not able to find any clear evidence of deformation twining significantly affecting the β RX texture [35]. In addition, here, it is shown that in the PSC samples, shear localisation tended to generate only one strong, rotated, parent grain component and resulted in a much lower level of grain refinement. In fact, the characteristic four-fold motif β RX micro-texture that was associated with annealing twinning in ref. [35] became more dominant under more homogeneous deformation conditions (e.g. at lower strain rates and higher temperatures, Fig. 8).

The lower ~50 μm β-grain size limit, seen across nearly all the samples that were deformed by more than ~14%, could largely be attributed to the rapid grain growth that occurs in the β phase field (Fig. 16), even though a relatively low peak temperature was used of ~100 °C above the β transus for the standard annealing treatment (1100 °C for 1 s). For example, in a related study on the effect of surface peening, it has been shown that rapid-heating β RX grain sizes below ~20 μm can be observed on re-heating just above the β transus [36]. However, annealing twinning only requires sufficient α-β interface defects to cause stacking faults to develop during re-growth of β, while it is still constrained between the dissolving α lamellar plates. This mechanism, therefore, does not require a large strain to develop the large local lattice rotations, which are a pre-requisite for conventional discontinuous RX, and it will also saturate at relatively low strains. In addition, it will be sensitive to heating rate because, due to the presence of multiple α-β interfaces and the thin nature of the volumes of retained β, defects generated in the β phase can readily recover. It should also be noted that, in such fine structures with the observed RX grain size, not many new grain nuclei are required relative to the enormous surface area of inter-lamellar residual β that existed within the original transformation structure, so that the formation of annealing twins following prior light deformation during the α → β transformation need only be a very rare event.

The absence of the characteristic four-fold motif in the texture from the sample deformed with a very coarse starting transformation microstructure, and the lack of formation of new highly misorientated grain orientations in this sample, despite the higher strain concentration in its centre, is also indirect evidence in favour of the annealing twinning theory. Indeed, this sample behaved much more as expected for a cold-deformed conventional Ti64 material, as it only partially recrystallized and largely developed subgrains at its centre, which agrees with other studies that suggest fine microstructure scaling tends to favour twinning when lattice defects are present during a phase transformation [40,50].

The grain size achieved by rapid-heating β RX was also shown to be insensitive to a reduction in deformation speed from 0.5 mm s^{-1} to 0.02 mm s^{-1} (Fig. 7), with a ~50 μm grain size measured for all samples under the same heating cycle. Similarly, the final RX β-grain size was shown to be insensitive to a deformation temperature increase up to 550 °C (Fig. 9). The insensitivity to these process parameter changes demonstrates that the final deformed microstructural state was not altered sufficiently to affect the final outcome; i.e. all samples deformed under this range of conditions and rapidly re-heated had an

adequate defect density to develop similar levels of new β orientations (or grain nuclei), probably by the annealing twinning mechanism, to be effectively indistinguishable after subsequent grain growth had occurred.

Ti64 exhibits significant strain-rate sensitivity at room temperature and a greater tendency for strain concentration was seen in the PSC tests at higher strain rates that caused earlier fracture, which is a problem that can be countered by elevating the deformation temperature [51]. Additionally, deforming at elevated temperatures reduces the critical resolved shear stresses (CRSSs) for HCP α Ti but, more importantly, the CRSS for ⟨c + a⟩ slip enabling more isotropic deformation. Both these process parameter dependencies were readily observed in the current work; i.e. reducing the deformation speed and elevating the deformation temperature produced more homogeneous RX across the PSC samples, implying a greater uniformity of deformation. For example, a surprisingly small rise in the deformation temperature to 350 °C was enough to significantly homogenise the strain distribution and maximise the β RX across the PSC samples. This could have useful implications to the WAAM process, as the strain distribution from cold rolling a non-flat deposit bead can be very heterogeneous [34].

Finally, when the scale of the starting transformation microstructure before deformation was varied by cooling samples from above the β transus with different rates, this had a significant effect on the sample texture and RX β-grain structure. When the starting α ILS was substantially reduced, greater shear concentration occurred in the PSC tests and there was an increase in the intensity of single texture shear components within the RX β grains. In addition, similar shear texture components dominated in the sample with the very coarse initial transformation microstructure that did not undergo RX at its centre. The coarse starting structure in this case, which was designed to replicate a more conventional material, prevented the twinning RX mechanism from operating, but some new HAGB orientations were observed to form within the intense 45° shear bands in this sample. Overall, this suggests two *separate* mechanisms contributed to the β RX in the PSC samples: the first probably occurs by annealing twinning in more uniformly deformed samples, which requires a fine transformation structure and a rapid heating rate to operate, and generates the unusual characteristic micro-texture with the four-fold symmetry in {001} pole figures; and a second that occurs if there is sufficient intense local shear to develop a high enough lattice rotation in the retained β matrix, to produce misorientated grain nuclei during re-growth of β on heating.

4.2. 4.2. β-grain growth

The inter-pass deformation WAAM simulations presented in this work demonstrated that with the standard rapid heating cycle employed, which exceeded the β transus by only 100 °C, a minimum β-grain size of ~50 μm could be achieved. However, it has been shown in related experiments on the effectiveness of inter-pass deformation using mechanical peening on grain refinement [36] that, in fact, the β-grain size increases dramatically with larger peak temperature rises after recrystallization, and the RX grain size has been found to be as fine as 20 μm at peak temperatures just above the β transus. The single thermal cycle employed for the simulations in the current work also does not include the accumulative effect of the full thermal history of a given deposited layer in a WAAM build, which typically involves 4–5 re-heating cycles above the β transus [22].

Here, the β-grain growth rates were measured isothermally following rapid heating in the dilatometer at temperatures of 1100, 1200, and 1300 °C (Fig. 17). To correlate these growth rates to previous studies on conventionally hot rolled Ti64 plate [39,41], the classical model in Eq. 1 was fitted to the data by assuming the grain size at $t = 0$ was zero. This approximation does not significantly affect the fitting constants and a good fit to the points was obtained using constants of: $n = 3.7$, $k = 7612\ \mathrm{m}^{3.7}\ \mathrm{s}^{-1}$, and $Q = 238\ \mathrm{kJ\ mol}^{-1}$, as can be seen in Fig. 17. This value of n is at the upper end of the normally reported range for grain growth exponents (e.g. 2–4 [40]), but the activation energy is more similar to that for diffusion of V, which is the slowest diffusing element present in Ti64 [52], than previously published [39,41]. In comparison, grain growth exponents of $n = 2$ have been determined in rolled Ti64 plate when isothermally annealed between 1030 and 1090 °C [39] and as high as $n = 4.6$ [41] under non-isothermal conditions. In these studies, higher activation energies (Q) were obtained of ~310 kJ mol^{-1}, and the difference in grain growth kinetics was proposed to be caused by strong textures affecting grain boundary mobility; i.e. in highly textured microstructures where, on average, there are more LAGBs, the grain growth kinetics are slower.

In the current work, rapid-heating β RX of deformed WAAM samples led to microstructures dominated by highly misorientated grains, characterised by the unique four-fold symmetry micro-texture motif seen in {001} pole figures, which had a weaker texture strength than that in the rolled plate studied in refs. [39,41] and this may be why we have obtained a more reasonable activation energy. Nevertheless, overall, from Figs. 15–17 it can be seen that the effect of grain growth on the final component grain size obtained by employing inter-pass rolling would be expected to be very significant. A rapid increase in grain size was found even for short heating cycles to peak temperatures that would be readily experienced by re-heating during the repeated passage of the heat source in the WAMM process. For example, using the grain growth law developed above, with a typical heating rate of ~650 °C, on heating close to the fusion boundary for 1 s, the temperature rise would be expected to lead to an increase in grain size from 20 μm to 320 μm. However, this law also shows that re-heating in subsequent passes, which would be to peak temperatures of the order of 200–300 °C below that reached in the first re-heating cycle [22], would have a very limited effect; i.e. the peak temperature reached in the first re-heating cycle will dominate the extent of grain growth and the final grain size. Limiting grain growth by controlling the first re-heating cycle after a layer is deposited and deformed would therefore be expected to be very important in achieving a finer RX β-grain size. This could, to some extent, be improved by more active thermal management; for example, by reducing the heat input or applying coolant, but this would also affect other aspects of the microstructure. Other options could include alloy modification to provide pining particles (e.g. the addition of Y into Ti64 has been shown to produce Y_2O_3 at β-grain boundaries which can retard growth [53]), however the introduction of such particles may also have negative consequences for mechanical performance.

5. Conclusions

The current work sought to determine the influence of the most important process parameters that affect the level of β recrystallization and the final grain size, when inter-pass deformation is employed to refine the coarse β-grain size normally seen in Ti64 components built using the WAAM process. Overall, it can be concluded that the level of β-grain refinement achieved by inter-pass deformation is insensitive to the range of deformation temperatures, deformation speeds, and changes to the as-deposited α + β microstructure that would be expected under the typical conditions associated with the WAAM process, provided a minimum compressive plastic strain is achieved in each added layer. Conversely, the final grain size was strongly affected by rapid grain growth on re-heating above the β transus. Therefore, the strain versus β-grain size plot in Fig. 4 and β-grain growth data in Fig. 17 can be used together as a process map to estimate the β-grain size in a given WAAM component. Overall, to achieve maximum β-grain refinement, the deposited material must be deformed to > 14% strain and grain growth must be limited as much as possible during further deposition passes.

The β recrystallization mechanism that gives rise to the beneficial development of a much reduced grain size and weak texture following

the application of relatively low deformation is still a matter of debate, but the data presented is consistent with previous results which suggest that, on rapidly heating fine deformed AM transformation microstructures, new β-grain orientations may be produced during the α → β transformation from the development of twinning faults at the transformation front.

The β RX grain size produced by rapid-heating was not strongly affected by a reduction of the initial fine α transformation microstructure, within the inter-lamellar spacing range typically found in AM processes. However, increasing the α plate spacing by using low cooling rates – comparable to those experienced in β annealed forged components – greatly reduced the level of recrystallization, and also appeared to change the recrystallization mechanism to favour fewer new β orientations as they were produced by lattice rotation. This latter, more conventional mechanism was much less efficient at refining the grain size.

Finally, it can be noted that it may be possible to utilise the rapid-heating β RX mechanism in conventionally produced Ti64 wrought components. Since grain refinement only requires a small amount of deformation and a subsequent rapid heating cycle, opportunities may exist to employ this RX mechanism locally at surfaces or in thin sheet materials.

Declaration of competing interest

The authors declare that they have no known competing financial interests or personal relationships that could have appeared to influence the work reported in this paper.

Acknowledgements

The authors are appreciative of the EPSRC grants (LightForm - EP/R001715/1; NEWAM – EP/R027218/1) and Innovate UK (Open Architecture Additive Manufacturing, OAAM) for supporting aspects of this research. P.B. Prangnell is also grateful to the Royal Academy of Engineering, UK, and Airbus for financial support through the Airbus-University of Manchester Centre for Metallurgical Excellence.

Data availability

The raw and processed data required to reproduce these findings cannot be shared at this time due to technical or time limitations.

References

[1] J. Allen, “An investigation into the comparative costs of additive manufacture vs. machine from solid for aero engine parts,” Proc. Meet. RTO-MP-AVT-139, pp. 17-1-17–10, 2006.
[2] G. Lütjering, J.C. Williams, Titanium, Springer, 2007.
[3] S. W. Williams, F. Martina, A. C. Addison, J. Ding, G. Pardal, and P. A. Colegrove, “Wire + arc additive manufacturing,” Mater. Sci. Technol.., vol. 32, no. 7, pp. 641–647, 2015.
[4] B. Baufeld, E. Brandl, O. Van Der Biest, Wire based additive layer manufacturing: comparison of microstructure and mechanical properties of Ti-6Al-4V components fabricated by laser-beam deposition and shaped metal deposition, J. Mater. Process. Technol. 211 (6) (2011) 1146–1158.
[5] K.M. Taminger, R.A. Hafley, Electron beam freeform fabrication for cost effective near-net shape manufacturing, Spec. Meet. Cost Eff. Manuf. via Net Shape Process. (NATO/RTO AVT-139), 16 2006, pp. 1–10.
[6] J. Gockel, J. Beuth, K.M. Taminger, Integrated control of solidification microstructure and melt pool dimensions in electron beam wire feed additive manufacturing of ti-6al-4v, Addit. Manuf 1 (2014) 119–126.
[7] F. Martina, P.A. Colegrove, S.W. Williams, J. Meyer, Microstructure of interpass rolled wire + arc additive manufacturing Ti-6Al-4V components, Metall. Mater. Trans. A Phys. Metall. Mater. Sci 46 (12) (2015) 6103–6118.
[8] F. Martina, J. Mehnen, S.W. Williams, P.A. Colegrove, F. Wang, Investigation of the benefits of plasma deposition for the additive layer manufacture of Ti-6Al-4V, J. Mater. Process. Technol. 212 (6) (2012) 1377–1386.
[9] T. Duda, L.V. Raghavan, 3D metal printing technology, IFAC-PapersOnLine 49 (29) (2016) 103–110.
[10] A.R. McAndrew, et al., Interpass rolling of Ti-6Al-4V wire + arc additively manufactured features for microstructural refinement, Addit. Manuf. 21 (March) (2018) 340–349.
[11] J.R. Hönnige, et al., Residual stress and texture control in Ti-6Al-4V wire + arc additively manufactured intersections by stress relief and rolling, Mater. Des. 150 (2018) 193–205.
[12] L. Neto, S. Williams, J. Ding, J. Hönnige, F. Martina, Advanced Surface Enhancement, Springer Singapore, Singapore, 2020.
[13] T. DebRoy, et al., Additive manufacturing of metallic components – process, structure and properties, Prog. Mater. Sci. 92 (2018) 112–224.
[14] C. Körner, Additive manufacturing of metallic components by selective electron beam melting - a review, Int. Mater. Rev. 61 (5) (2016) 361–377.
[15] I.A. Roberts, C.J. Wang, R. Esterlein, M. Stanford, D.J. Mynors, A three-dimensional finite element analysis of the temperature field during laser melting of metal powders in additive layer manufacturing, Int. J. Mach. Tools Manuf. 49 (12–13) (2009) 916–923.
[16] V.D. Fachinotti, A. Cardona, B. Baufeld, O. Van Der Biest, Finite-element modelling of heat transfer in shaped metal deposition and experimental validation, Acta Mater. 60 (19) (2012) 6621–6630.
[17] X. Bai, et al., Numerical analysis of heat transfer and fluid flow in multilayer deposition of PAW-based wire and arc additive manufacturing, Int. J. Heat Mass Transf. 124 (2018) 504–516.
[18] S.M. Kelly, S.L. Kampe, Microstructural evolution in laser-deposited multilayer Ti-6Al-4V builds: part II. Thermal modeling, Metall. Mater. Trans. A 35 (June) (2004) 1869–1879.
[19] S.M. Kelly, S.L. Kampe, Microstructural evolution in laser-deposited multilayer Ti-6Al-4V builds: part I. thermal modeling, Metall. Mater. Trans. A Phys. Metall. Mater. Sci. 35 A (6) (2004) 1869–1879.
[20] J. Donoghue, A.A. Antonysamy, F. Martina, P.A. Colegrove, S.W. Williams, P.B. Prangnell, The effectiveness of combining rolling deformation with wire-arc additive manufacture on β-grain refinement and texture modification in Ti-6Al-4V, Mater. Charact. 114 (2016) 103–114.
[21] P. Åkerfeldt, M.L. Antti, R. Pederson, Influence of microstructure on mechanical properties of laser metal wire-deposited Ti-6Al-4V, Mater. Sci. Eng. A 674 (2016) 428–437.
[22] A. Ho, H. Zhao, J.W. Fellowes, F. Martina, A.E. Davis, P.B. Prangnell, On the origin of microstructural banding in Ti-6Al4V wire-arc based high deposition rate additive manufacturing, Acta Mater. 166 (2019).
[23] F. Wang, S.W. Williams, P.A. Colegrove, A.A. Antonysamy, Microstructure and mechanical properties of wire and arc additive manufactured Ti-6Al-4V, Metall. Mater. Trans. A Phys. Metall. Mater. Sci 44 (2) (2013) 968–977.
[24] X. Zhang, F. Martina, J. Ding, X. Wang, S.W. Williams, Fracture toughness and fatigue crack growth rate properties in wire + arc additive manufactured Ti-6Al-4V, Fatigue Fract. Eng. Mater. Struct. 40 (5) (2017) 790–803.
[25] D. Ding, Z. Pan, D. Cuiuri, H. Li, Wire-feed additive manufacturing of metal components: technologies, developments and future interests, Int. J. Adv. Manuf. Technol. 81 (1–4) (2015) 465–481.
[26] H. Zhao, A. Ho, A.E. Davis, A.A. Antonysamy, P.B. Prangnell, Automated image mapping and quantification of microstructure heterogeneity in additive manufactured Ti6Al4V, Mater. Charact. 147 (July 2018) (2019) 131–145.
[27] P.A. Kobryn, S.L. Semiatin, Microstructure and texture evolution during solidification processing of Ti-6A1-4V, J. Mater. Process. Technol. 135 (2–3 SPEC) (2003) 330–339.
[28] R. Filip, K. Kubiak, W. Ziaja, J. Sieniawski, The effect of microstructure on the mechanical properties of two-phase titanium alloys, J. Mater. Process. Technol. 133 (1–2) (2003) 84–89.
[29] T. Ahmed, H.J. Rack, Phase transformations during cooling in alpha + beta titanium alloys, Mater. Sci. Eng. A 243 (1998) 206–211.
[30] M.J. Bermingham, S.D. McDonald, M.S. Dargusch, D.H. St.John, Grain-refinement mechanisms in titanium alloys, J. Mater. Res. 23 (1) (2008) 97–104.
[31] M.J. Bermingham, S.D. McDonald, D.H. StJohn, M.S. Dargusch, Segregation and grain refinement in cast titanium alloys, J. Mater. Res. 24 (4) (2009) 1529–1535.
[32] T. Lyman, Atlas of Microstructures of Industrial Alloys, American Society for Metals, 1972.
[33] A.A. Antonysamy, J. Meyer, P.B. Prangnell, Effect of build geometry on the β-grain structure and texture in additive manufacture of Ti6Al4V by selective electron beam melting, Mater. Charact. 84 (2013) 153–168.
[34] F. Martina, S.W. Williams, P.A. Colegrove, Improved microstructure and increased mechanical properties of additive manufacture produced Ti-6Al-4V by interpass cold rolling, SFF Symp, 2013, pp. 490–496.
[35] J. Donoghue, et al., On the observation of annealing twins during simulating β-grain refinement in Ti-6Al-4V high deposition rate AM with in-process deformation, Acta Mater. 186 (2019) 229–241.
[36] J.R. Hönnige, et al., The Effectiveness of Grain Refinement by Machine Hammer Peening in High Deposition Rate Wire-Arc AM Ti-6Al-4V, Under Rev (2020).
[37] ASM International, Materials Properties Handbook: Titanium Alloys, Materials Park, OH, 1994.
[38] J. R. Hönnige, P. A. Colegrove, P. B. Prangnell, A. Ho, and S. W. Williams, “The Effect of Thermal History on Microstructural Evolution, Cold-Work Refinement and α/β Growth in Ti-6Al-4V Wire + Arc AM,” pp. 1–25.
[39] S.L. Semiatin, J.C. Soper, I.M. Sukonnik, Short-time beta grain growth conventional kinetics alloy, Acta Metall. 44 (5) (1996) 1979–1986.
[40] F.J. Humphreys, M. Hatherly, Recrystallization and Related Annealing Phenomena, Elsevier, Oxford, 1996.
[41] S.L. Semiatin, P.N. Fagin, M.G. Glavicic, I.M. Sukonnik, O.M. Ivasishin, Influence on texture on beta grain growth during continuous annealing of Ti-6Al-4V, Mater. Sci. Eng. A 299 (1–2) (2001) 225–234.

[42] M. Abbaszadeh, et al., Numerical investigation of the effect of rolling on the localized stress and strain induction for wire + arc additive manufactured structures, J. Mater. Eng. Perform. 28 (8) (2019) 4931–4942.
[43] A.N. Levanov, Improvement of metal forming processes by means of useful effects of plastic friction, J. Mater. Process. Technol. 72 (2) (1997) 314–316.
[44] C. Bandini, B. Reggiani, L. Donati, L. Tomesani, Code validation and development of user routines for microstructural prediction with Qform, Mater. Today Proc 2 (10) (2015) 4904–4914.
[45] P.S. Davies, An Investigation of Microstructure and Texture Evolution in the Near-α Titanium Alloy Timetal 834, University of Sheffield, 2009.
[46] P.S. Davies, B.P. Wynne, W.M. Rainforth, M.J. Thomas, P.L. Threadgill, Development of microstructure and crystallographic texture during stationary shoulder friction stir welding of Ti-6Al-4V, Metall. Mater. Trans. A Phys. Metall. Mater. Sci 42 (8) (2011) 2278–2289.
[47] M. Humbert, N. Gey, The calculation of a parent grain orientation from inherited variants for approximate (b.c.c.-h.c.p.) orientation relations, J. Appl. Crystallogr. 35 (4) (2002) 401–405.
[48] N. Gey, M. Humbert, Specific analysis of EBSD data to study the texture inheritance due to the β→α phase transformation, J. Mater. Sci. 38 (6) (2003) 1289–1294.
[49] S. Mishra, T. DebRoy, Measurements and Monte Carlo simulation of grain growth in the heat-affected zone of Ti-6Al-4V welds, Acta Mater. 52 (5) (2004) 1183–1192.
[50] J. Wang, Z. Zeng, C.R. Weinberger, Z. Zhang, T. Zhu, S.X. Mao, In situ atomic-scale observation of twinning-dominated deformation in nanoscale body-centred cubic tungsten, Nat. Mater. 14 (6) (2015) 594–600.
[51] A. El-Domiaty, The effect of strain, strain rate and temperature on formability of Ti-6Al-4V alloy, J. Mater. Process. Tech 32 (1–2) (1992) 243–251.
[52] W.F. Gale, T.C. Totemeier (Eds.), Smithells Metals Reference Book, 8th ed., Elsevier, Oxford, 2004.
[53] G.C. Obasi, S. Birosca, J. Quinta Da Fonseca, M. Preuss, Effect of β grain growth on variant selection and texture memory effect during α → β → α phase transformation in Ti-6 Al-4 v, Acta Mater. 60 (3) (2012) 1048–1058.

2020-03-28

The effect of processing parameters on þÿ r a p i d - h e a t i n g ² r e c r y s t a l l i z a t i inter-pass deformed Ti-6Al-4V wire-arc additive manufacturing

Davis, Alec E.

Elsevier

Davis AE, Kennedy JR, Ding J, Prangnell PB. (2020) The effect of processing parameters on þÿ r a p i d - h e a t i n g ² r e c r y s t a l l i z a t i o n i n i n t e r - p a s s d e f o r m e d T i - 6 A l - 4 V w i r e - a manufacturing. Materials Characterization, Volume 163, May 2020, Article number 110298

https://doi.org/10.1016/j.matchar.2020.110298